

NAVAL RESEARCH LABORATORY NAVAL CENTER FOR SPACE TECHNOLOGY

Error Budget Document
for the
Full-Sky Astrometric Mapping Explorer (FAME)

NCST-D-FMXXX

11 December 2000

Approved By: _____ Date: _____
Dr. Kenneth J. Johnston, Principle Investigator, USNO

Approved By: _____ Date: _____
Mark S. Johnson, Program Manager, NRL Code 8122

Approved By: _____ Date: _____
Dr. Richard Vassar, Program Manager, Lockheed Martin Advanced Technology Center

Approved By: _____ Date: _____
Dr. Scott Horner, Chief Systems Engineer, Lockheed Martin Advanced Technology Center

Approved By: _____ Date: _____
Ralph Gaume, MO&DA Lead, USNO

Approved By: _____ Date: _____
, NRL

DISTRIBUTION STATEMENT C: Distribution authorized to U.S. Government agencies and their contractors; Administrative or Operational Use. Other requests for this document shall be referred to Mr. M. Johnson, Code 8133, Naval Research Laboratory, 4555 Overlook Avenue, S.W., Washington, D.C. 20375-5000.

**4555 Overlook Avenue, S.W.
Washington, D.C. 20375-5000**

TABLE OF CONTENTS

Section	Title	Page
1.	INTRODUCTION	1-1
1.1	Identification.....	1-1
1.2	Purpose.....	1-1
1.3	Observatory Overview.....	1-1
1.3.1	Science Objectives.....	1-1
1.3.2	Observatory.....	1-1
1.4	Document Overview.....	1-1
2.	REFERENCED DOCUMENTS	2-1
2.1	Government Documents.....	2-1
2.1.1	Specifications.....	2-1
2.1.2	Standards.....	2-1
2.1.3	Other Publications.....	2-1
2.2	Non-Government Documents.....	2-1
2.2.1	Specifications.....	2-1
2.2.2	Standards.....	2-1
2.2.3	Other Publications.....	2-1
3.	ERROR BUDGET TREE (9TH MAGNITUDE STAR).....	3-1
3.1	Science Requirments.....	3-1
3.2	Astrometry, Single Observation.....	3-2
3.3	Unbinned Cross-Scan Motion.....	3-3
3.4	Astrometry, Mission.....	3-4
3.5	Photometric Errors, Single Observation.....	3-5
3.6	Photometric, Mission.....	3-5
3.7	Data Windows.....	3-6
3.8	Acquisition Mode.....	3-7
4.	ERROR BUDGET DESCRIPTION.....	4-1
4.1	Science Requirements.....	4-1
4.2	Astrometry, Single Observation Error, In-Scan.....	4-1
4.2.1	Random.....	4-2
4.2.1.1	Photon Noise.....	4-2
4.2.1.2	Read Noise.....	4-2
4.2.1.2.1	CCD Read Noise.....	4-2
4.2.1.2.2	Electronics Read Noise.....	4-2
4.2.1.3	Dark Current.....	4-2
4.2.1.4	Cosmic Rays.....	4-3
4.2.2	TDI Error.....	4-3
4.2.2.1	Rotation Rate Determination Error.....	4-3
4.2.2.2	TDI Rate Mismatch.....	4-3
4.2.2.2.1	TDI Setting Resolution.....	4-4
4.2.2.2.2	S/C Rotation Rate Drift.....	4-4
4.2.2.3	Oscillator Stability.....	4-4
4.2.2.4	Optical Distortion.....	4-4
4.2.3	Dynamical Perturbations.....	4-4
4.2.3.1	Stochastic and Other Hard To Model Dynamical Perturbations.....	4-4
4.2.3.1.1	Fuel Sloshing.....	4-5
4.2.3.1.2	Earth Radiation Pressure.....	4-5
4.2.3.1.3	Variability of Solar Irradiance.....	4-5
4.2.3.1.4	Nutation Damping Mechanism Stiction and/or Other Undesirable Behaviors.....	4-5

4.2.3.2	Solar Shield Dynamical Perturbations.....	4-5
4.2.3.2.1	Shield (Panels, Teflon Tape, Webbing, Etc.) and Flattop Albedos.....	4-5
4.2.3.2.2	Variations In Effective Shield Angle.....	4-5
4.2.3.2.3	Shield Component Geometry Perturbations.....	4-5
4.2.3.2.4	Thermal Radiation Emission Torques.....	4-6
4.2.3.2.5	Axis of Shield Misaligned With Spacecraft Spin Axis.....	4-6
4.2.3.2.6	Trim Tab Problems.....	4-6
4.2.3.3	Dynamical Perturbations Due To Events.....	4-6
4.2.3.3.1	Eclipses.....	4-6
4.2.3.3.2	Geotail Particle Bursts.....	4-6
4.2.3.3.3	Magnetopause Crossings.....	4-6
4.2.3.3.4	Micrometeoroid Hits.....	4-6
4.2.3.4	Other Smooth Dynamical Perturbations.....	4-6
4.2.3.4.1	Precession Variation.....	4-7
4.2.3.4.2	Aberration Variation.....	4-7
4.2.3.4.3	Gravity Gradient Torques.....	4-7
4.2.3.4.4	Magnetic Torques.....	4-8
4.2.3.4.5	Movement of Center of Gravity As Fuel is Expended.....	4-8
4.2.3.4.6	Variations of Instantaneous Sun Direction Due to sun Tracking Dynamics.....	4-8
4.2.3.4.7	Variation of Solar Radiation Pressure As Spacecraft Orbits Around the Earth.....	4-8
4.2.3.4.8	Lunar, Solar, and Planetary Gravitational Torques.....	4-8
4.2.4	This section intentionally blank.....	4-8
4.2.5	PSF Knowledge.....	4-8
4.2.5.1	Stellar Spectrum.....	4-8
4.2.5.2	Start-Stop Technology ($V < 9$).....	4-9
4.2.5.3	Optical Effect on PSF.....	4-9
4.2.5.4	Confusion.....	4-9
4.2.6	Spacecraft Tracking.....	4-9
4.2.6.1	Unmodeled Velocity Perturbations.....	4-9
4.2.6.2	S/C Position Knowledge.....	4-9
4.2.6.3	Ground Station Position.....	4-9
4.2.6.4	Time Knowledge.....	4-9
4.2.7	Optics.....	4-10
4.2.7.1	Stray Light.....	4-10
4.2.7.1.1	Earth.....	4-10
4.2.7.1.2	Moon.....	4-10
4.2.7.1.3	Bright Stars/Planets.....	4-10
4.2.7.1.4	Sun.....	4-10
4.2.7.1.5	Other Background.....	4-10
4.2.7.2	Aberration, Including Distortion.....	4-10
4.2.7.3	Opto-Thermal-Mechanical Stability.....	4-10
4.2.7.4	Chromatic Errors.....	4-10
4.2.8	CCD and Electronics.....	4-10
4.2.8.1	Charge Spreading.....	4-10
4.2.8.2	Charge Transfer Inefficiency (CTI).....	4-10
4.2.8.3	Wavelength Dependence of Absorption.....	4-10
4.2.8.4	Quantum Efficiency Variation.....	4-11
4.2.8.5	Amplifier Gain Stability.....	4-11
4.2.8.6	Linearity.....	4-11
4.3	Unbinned Cross-Scan Motion.....	4-11
4.3.1	Dynamical Perturbations.....	4-11
4.3.1.1	Stochastic and Other Hard-to-Model Dynamical Perturbations.....	4-11
4.3.1.1.1	Fuel Sloshing.....	4-11
4.3.1.1.2	Earth Radiation Pressure.....	4-12

4.3.1.1.3 Variability of Solar Irradiance..... 4-12

4.3.1.1.4 Nutation Damping Mechanism Stiction and/or Other Undesirable Behaviors..... 4-12

4.3.1.2 Solar Shield Dynamical Perturbations..... 4-12

4.3.1.2.1 Shield (Panels, Teflon Tape, Webbing, Etc.) and Flattop Albedos..... 4-12

4.3.1.2.2 Variations In Effective Shield Angle..... 4-12

4.3.1.2.3 Shield Component Geometry Perturbations..... 4-12

4.3.1.2.4 Thermal Radiation Emission Torques..... 4-12

4.3.1.2.5 Axis of Shield Misaligned With Spacecraft Spin Axis..... 4-12

4.3.1.2.6 Trim Tab Problems..... 4-12

4.3.1.3 Dynamical Perturbations Due to Events..... 4-12

4.3.1.3.1 Eclipses..... 4-12

4.3.1.3.2 Geotail Particle Bursts..... 4-12

4.3.1.3.3 Magnetopause Crossings..... 4-12

4.3.1.3.4 Micrometeoroid Hits..... 4-13

4.3.1.4 Other Smooth Dynamical Perturbation..... 4-13

4.3.1.4.1 Precession Variation..... 4-13

4.3.1.4.2 Aberration Variation..... 4-13

4.3.1.4.3 Gravity Gradient Torques..... 4-13

4.3.1.4.4 Magnetic Torques..... 4-13

4.3.1.4.5 Movement of Center of Gravity As Fuel Is Expended..... 4-13

4.3.1.4.6 Variations of Instantaneous Sun Direction Due to Sun Tracking Dynamics..... 4-13

4.3.1.4.7 Variation of Solar Radiation Pressure As Spacecraft Orbits Around the Earth..... 4-13

4.3.1.4.8 Lunar, Solar, and Planetary Gravitational Torques..... 4-13

4.3.2 Random..... 4-13

4.3.3 Cross-Scan Jitter..... 4-13

4.3.4 Optics..... 4-13

4.3.4.1 Stray Light..... 4-13

4.3.4.1.1 Earth..... 4-13

4.3.4.1.2 Moon..... 4-13

4.3.4.1.3 Bright Stars/Planets..... 4-13

4.3.4.1.4 Sun..... 4-14

4.3.4.1.5 Other Background..... 4-14

4.3.4.2 Optical Distortion..... 4-14

4.3.4.3 Other Optical Aberrations..... 4-14

4.3.4.4 Opto-Thermal-Mechanical Stability..... 4-14

4.3.4.5 Chromatic Errors..... 4-14

4.3.5 CCD and Electronics..... 4-14

4.3.5.1 Photon Noise..... 4-14

4.3.5.2 Read Noise..... 4-14

4.3.5.2.1 CCD Read Noise..... 4-14

4.3.5.2.2 Electronics Read Noise..... 4-14

4.3.5.3 Quantum Efficiency Variation..... 4-14

4.3.5.4 Charge Transfer Inefficiency (CTI)..... 4-14

4.3.5.5 Dark Current..... 4-15

4.3.5.6 Star Color Variation..... 4-15

4.3.5.7 Charge Spreading..... 4-15

4.3.5.8 Amplifier Gain Stability..... 4-15

4.3.5.9 Linearity..... 4-15

4.3.5.10 Cosmic Rays..... 4-15

4.4 Astrometry, Mission..... 4-15

4.4.1 Number of Observations..... 4-15

4.4.1.1 Confusion..... 4-15

4.4.1.2 Eclipses..... 4-15

4.4.1.3 Occultations..... 4-16

4.4.1.4	Bright Stars/Scattered Light.....	4-16
4.4.1.5	Cosmic Rays.....	4-16
4.4.1.6	Bad Columns.....	4-16
4.4.2	Scanning Geometry.....	4-16
4.4.2.1	Nominal Sun Angle.....	4-16
4.4.2.2	Precession Rate.....	4-16
4.4.2.3	Spin Rate.....	4-16
4.4.3	Single-Observation Error.....	4-17
4.4.4	Optics.....	4-17
4.4.4.1	Basic Angle Stability.....	4-17
4.4.4.1.1	Compound Mirror Stability.....	4-17
4.4.4.1.2	Twisting of Other Optical Elements.....	4-17
4.4.5	S/C Tracking.....	4-17
4.4.5.1	S/C Position.....	4-17
4.4.5.2	Gound Station Position.....	4-17
4.4.5.3	Time Knowledge.....	4-17
4.4.6	Instrument Parameter Calibrations.....	4-17
4.5	Photometry, Single Observation.....	4-17
4.5.1	Astrometric CCDs.....	4-17
4.5.1.1	Random.....	4-18
4.5.1.1.1	Photon Noise.....	4-18
4.5.1.1.2	Read Noise.....	4-18
4.5.1.1.3	Dark Current.....	4-18
4.5.1.2	Stellar Variability.....	4-18
4.5.1.3	Confusion.....	4-18
4.5.1.4	Stray Light.....	4-18
4.5.1.5	Optics.....	4-18
4.5.1.5.1	Aging of Optical Coatings.....	4-18
4.5.1.6	CCD and Electronics.....	4-18
4.5.1.6.1	DC Level.....	4-18
4.5.1.6.2	QE Variations.....	4-19
4.5.1.6.3	CTI Effects.....	4-19
4.5.1.6.4	Star Color Variation.....	4-19
4.5.1.6.5	Charge Spreading.....	4-19
4.5.1.6.6	Linearity.....	4-19
4.5.1.6.7	Amplifier Gain Stability.....	4-19
4.5.1.6.8	Charge Traps.....	4-19
4.5.2	SDSS Filters.....	4-19
4.5.3	Sloan Filters.....	4-19
4.6	Photometry, Mission.....	4-19
4.6.1	Astrometric CCDs.....	4-19
4.6.1.1	Calibration of Standard Stars.....	4-20
4.6.1.2	Stellar Variability.....	4-20
4.6.2	SDSS Filters.....	4-20
4.6.2.1	Standard Candles.....	4-20
4.6.2.2	Ground Calibration of Passbands.....	4-20
4.6.2.3	Stellar Variability.....	4-20
4.6.3	Sloan Filters.....	4-20
4.7	Data Windows.....	4-20
4.7.1	Input Catalog.....	4-21
4.7.1.1	Catalog Error.....	4-21
4.7.1.2	Proper Motion Error.....	4-21
4.7.1.2.1	Proper Motion in the Catalog Epoch.....	4-21
4.7.1.2.2	Proper Motion in the Current Epoch Relative to the Catalog Epoch.....	4-21

4.7.2 On-Board Calculation..... 4-21

4.7.2.1 Distortion..... 4-21

4.7.2.2 Estimates of Cross-Scan Trajectory..... 4-21

4.7.2.3 Aberrations..... 4-21

4.7.2.4 Chromatic Effects..... 4-21

4.7.2.5 Pixelization..... 4-21

4.7.2.6 Location of the CCDs..... 4-22

4.7.2.7 On-Board Attitude Determination..... 4-22

4.7.2.8 On-Board Centering..... 4-22

4.8 Acquisition Mode..... 4-22

4.8.1 Star Tracker to Instrument Boresight..... 4-22

4.8.2 Star Tracker Accuracy..... 4-22

4.8.3 Locations of CCDs..... 4-22

5. NOTES..... 5-1

5.1 Definitions..... 5-1

5.2 Acronyms and Abbreviations..... 5-2

5.3 List of Open Items..... 5-3

DRAFT

LIST OF FIGURES

Number	Title	Page
Figure 3-1.....		3-1
Figure 3-2.....		3-2
Figure 3-3.....		3-3
Figure 3-4.....		3-4
Figure 3-5.....		3-5
Figure 3-6.....		3-5
Figure 3-7.....		3-6
Figure 3-8.....		3-7

DRAFT

LIST OF TABLES

Number	Title	Page
Table 4-1.	Blur Sources (TBD).....	4-3
Table 4-2.	Clock Stability	4-4

DRAFT

1. INTRODUCTION

1.1 Identification.

This document applies to the Full-sky Astrometric Mapping Explorer (FAME) Observatory program, a NASA Medium Class (MIDEX) Explorer mission.

1.2 Purpose.

The purpose of this document is to describe the error sources considered in the FAME design, describe the values estimated for those error sources and how those values were determined, and describe how the different error sources combine to determine the total mission errors.

This document is intended as a guide for determining the mission, spacecraft, and instrument requirements described in the *Mission Requirements Document*, *Spacecraft Requirements Document*, and *Instrument Requirements Document*.

1.3 Observatory Overview.

FAME will provide the positions, proper motions, parallaxes, and photometry of nearly all stars as faint as 15th visual magnitude with accuracies of 0.24 nanoradians (50 microarcseconds [μas]) at 9th visual magnitude and 2.4 nanoradians (500 μas) at 15th visual magnitude. Stars will be observed with the Sloan Digital Sky Survey g' , r' , i' , and z' filters for photometric magnitudes. The data are acquired by a scanning survey instrument evolved from the *Hipparcos* mission with a mission life of 2.5 years and an extended mission to 5 years.

1.3.1 Science Objectives.

Primary science requirements are fully described in the document *FAME Science Requirements*. The primary science requirements are summarized below.

FAME will create a catalog of star positions based on a 2 1/2 year mission with:

1. A measured position, parallax, and proper motion of stars between 5th to 9th visual magnitude to 50 microarcseconds, 50 microarcseconds, and 70 microarcseconds per year respectively. For stars fainter than 9th visual magnitude the mission astrometric accuracy shall degrade no more rapidly than implied by the photon statistics, i.e. no more rapidly than the inverse square root of the apparent brightness. At 15th visual magnitude, the mission astrometric accuracy shall be no worse than 500 microarcseconds.
2. Photometric magnitudes for all stars in the wide band astrometric bandpass as well as the Sloan g' , r' , i' , and z' filters.
3. The accuracy of individual observation magnitudes will be from millimagnitudes at 9th magnitude to four hundredths magnitude at 15th magnitude. The mission magnitude accuracies will be tenths of a millimagnitude at 9th magnitude and five millimagnitudes at 15th magnitude.
4. The above accuracy specifications apply to 90% of the unconfused sources at a given magnitude, with the other 10% not exceeding twice the accuracy specification. The coverage is for > 98% of the sky to take into account areas of crowding.

1.3.2 Observatory.

The FAME observatory consists of a spacecraft bus and a single instrument subsystem. The spacecraft bus will be designed and fabricated at the Naval Research Laboratory. The instrument will be designed and fabricated at the Lockheed Martin Space Systems Advanced Technology Center. The U.S. Naval Observatory will provide overall project supervision as well as Mission Operations and Data Analysis for the lifetime of the mission.

1.4 Document Overview.

The requirements in this document flow down from the Mission Requirements Document (MRD), the MIDEX Assurance Requirements (MAR), and the FAME Science Requirements Document. This document is organized as follows:

Section 1, *Scope*: The purpose and contents of this document.

Section 2, *Referenced Documents*: A list of documents referenced in or required for use with this document.

Section 3, *Error budget trees*: The error budget trees showing the individual error sources and how they combine to produce the required mission accuracy.

Section 4, *Error budget descriptions*: This section provides a detailed description of what is included in each of the error boxes and how the values and error bars were derived.

Section 5, *Notes*: Includes a list of definitions of terms, a list of acronyms and abbreviations used in this document and until final release at CDR a list of open requirements (those with “TBD” or “TBR”), and the planned closure of each.

DRAFT

2. REFERENCED DOCUMENTS

The following documents of the version indicated form a part of this specification to the extent indicated herein. In the event of conflict between the documents referenced herein and the contents of this specification, the contents of this specification shall be considered a superseding requirement until the conflict is resolved.

Following the name of each document is an abbreviation. This is the name used in the text of this specification to refer to a document in this list. In every case where a reference is made in a requirements statement, the reference shall include the paragraph number in the source document. Any reference which does not contain a paragraph number is assumed to refer to the entire document.

2.1 Government Documents.

2.1.1 Specifications.

Number	Title	Date	Paragraph Ref.
NCST-D-FM002	FAME Mission Requirements Document (MRD)	8 May 2000	
NCST-	FAME Spacecraft to Instrument ICD (S/C_ICD)	TBR	
NCST-	FAME Science Requirements Document (SRD)	TBR	
GSFC-410-MIDEX-003	MIDEX Quality Assurance Requirements (MAR)	TBR	

2.1.2 Standards.

2.1.3 Other Publications.

2.2 Non-Government Documents.

2.2.1 Specifications.

2.2.2 Standards.

2.2.3 Other Publications.

Author	Title	Publisher
Wertz and Larson	Space Mission Analysis and Design, 3 rd Edition	Microcosm Press and Kluwer Academic Publishers, El Segundo, CA, 1999

DRAFT

3. ERROR BUDGET TREE (9TH MAGNITUDE STAR)

The FAME Observatory is a spinning telescope continuously observing the sky. As the Observatory rotates, it uses the two fields of view of the telescope to image the sky onto a focal plane populated with CCDs operated in TDI (drift scan) mode. The Observatory acquires data on both the astrometric (position) and photometric (brightness as a function of color) properties of the stars in the field of view. FAME will observe each of the 40 million stars in its input catalog on the order of 1000 times each during the course of the mission lifetime. These single observations will be combined together into a rigid astrometric reference frame and a catalog of photometric magnitudes. The astrometric error budget is therefore broken down into the astrometric, single observation errors (§3.2) and errors in the astrometry for the mission (§3.4) after the single observations have been combined together. The photometric error budget is similarly structured with single observation errors in errors in §3.5 and photometric errors for the mission in §3.6. Section 3.3 consists of two components, one being the control of the cross-scan motion allowable to prevent over-smearing of the PSF in the cross-scan dimension and to keep the star’s PSF within the data collection window. The second component is the knowledge of the cross-scan attitude required for the mission astrometric solution. Sections 3.7 and 3.8 capture other requirements that must be met for the mission to achieve its objectives but do not directly contribute to the overall mission errors.

3.1 Science Requirements.

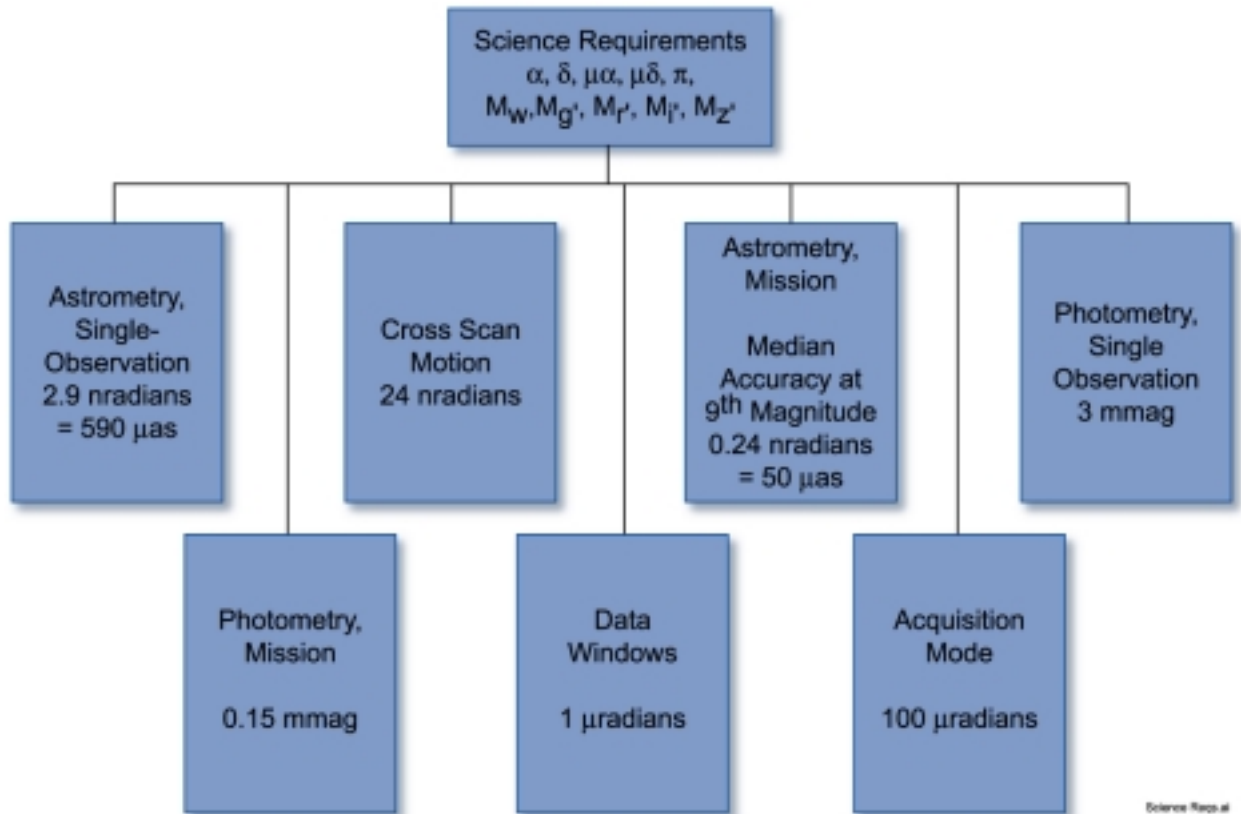


Figure 3–1.

The top level error budget flowdown from the science requirements (α = position in the sky in right ascension, δ = position in the sky in declination, $\mu\alpha$ = proper motion in right ascension, $\mu\delta$ = proper motion in declination, π = parallax, m_w = photometric brightness in the astrometric band, $m_{g'}$ = photometric brightness in the g' band, $m_{r'}$ = photometric brightness in the r' band, $m_{i'}$ = photometric brightness in the i' band, $m_{z'}$ = photometric brightness in the z' band). The full interconnectivity of the errors is not shown in this diagram. For example, the mission photometric accuracy will couple into the astrometric error budget if PSF modeling centering is used.

3.2 Astrometry, Single Observation Error, In-Scan.

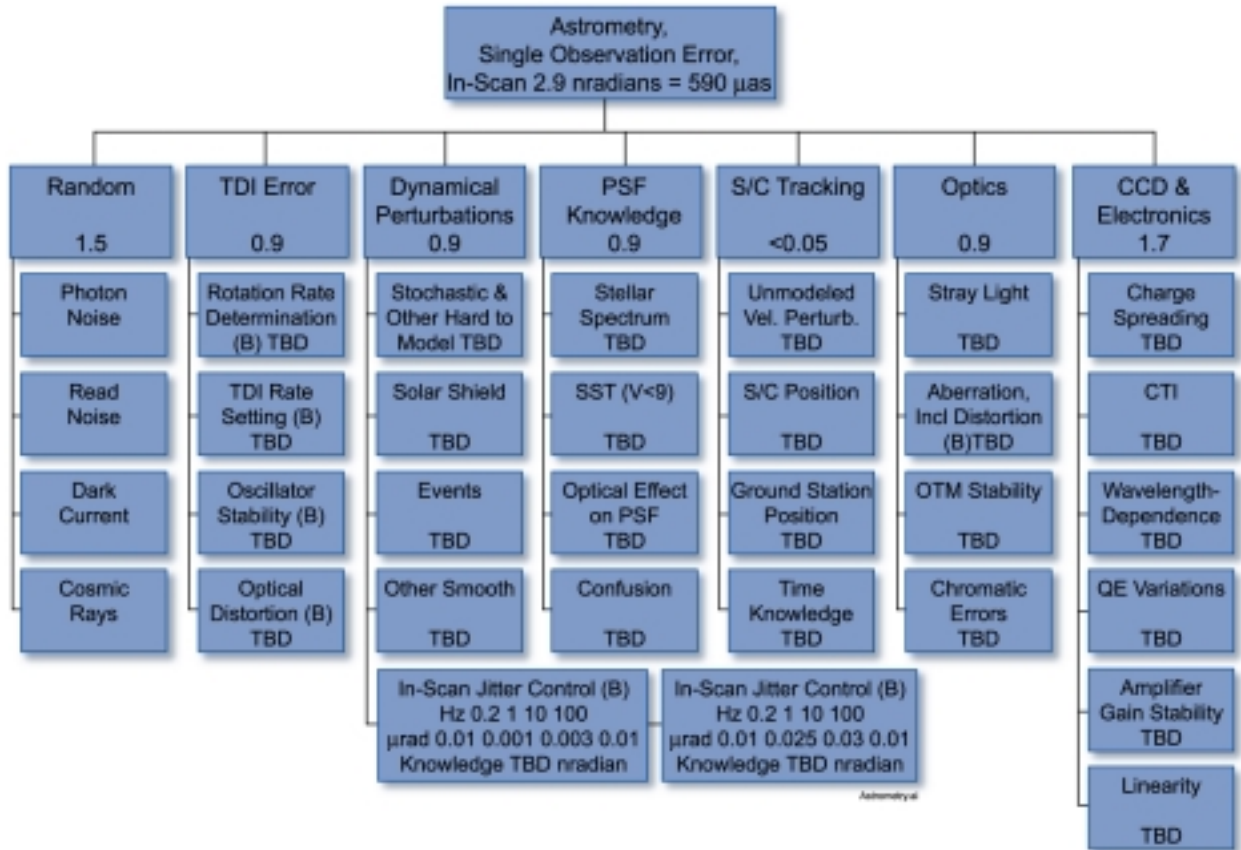


Figure 3–2.

Errors for astrometry, for single observations in the in-scan direction. Errors are given in nanoradians.

3.3 Unbinned Cross-Scan Motion.

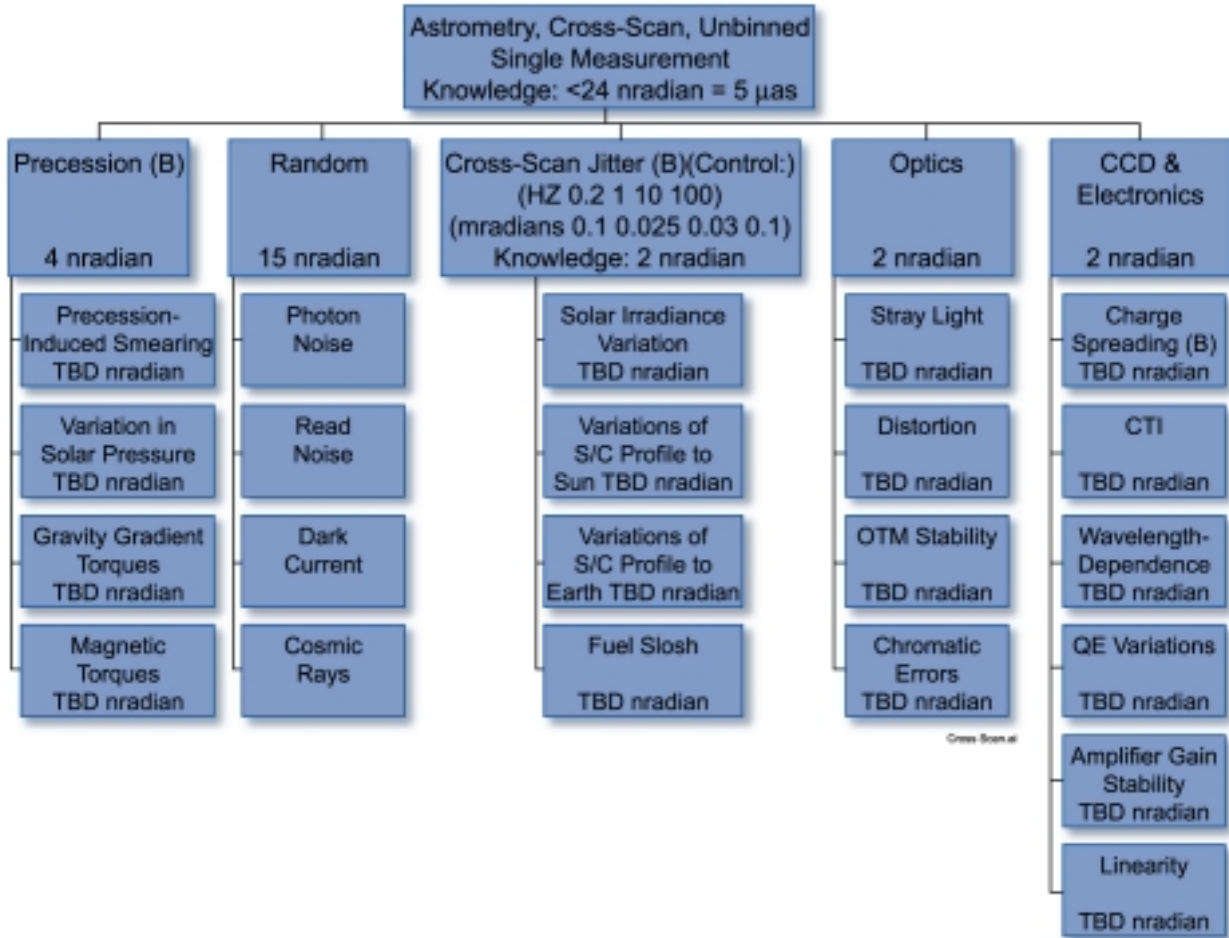


Figure 3-3.

Requirements for cross-scan direction attitude control and knowledge. Note that this tree differs from the rest of this document in listing requirements, not astrometric error. The error corresponding to the net motion allowed by these requirements is given in the box "Cross-scan Motion" in Figure 3-2. "Knowledge" is defined in this table as the ability to center on unbinned stars for single observations. Control requirements are in parentheses. The knowledge requirement only applies to grid stars.

3.4 Astrometry, Mission.

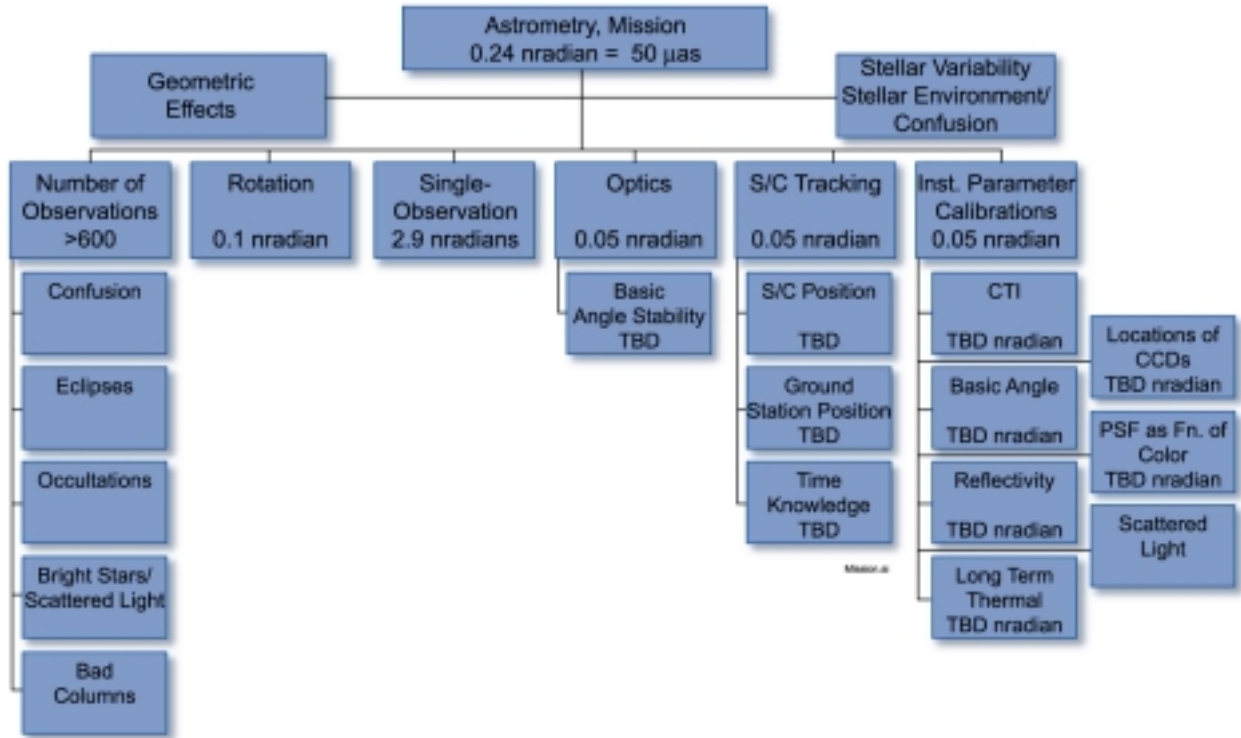


Figure 3-4.

Mission error, for position in the final catalog. Units are nradian. Note that single-observation error dominates. In the FAME Concept Study Report, the allowance for the remainder, systematic error that fails to average down, was 10 μas = 0.05 nradian added in RSS.

3.5 Photometric Errors, Single Observation.

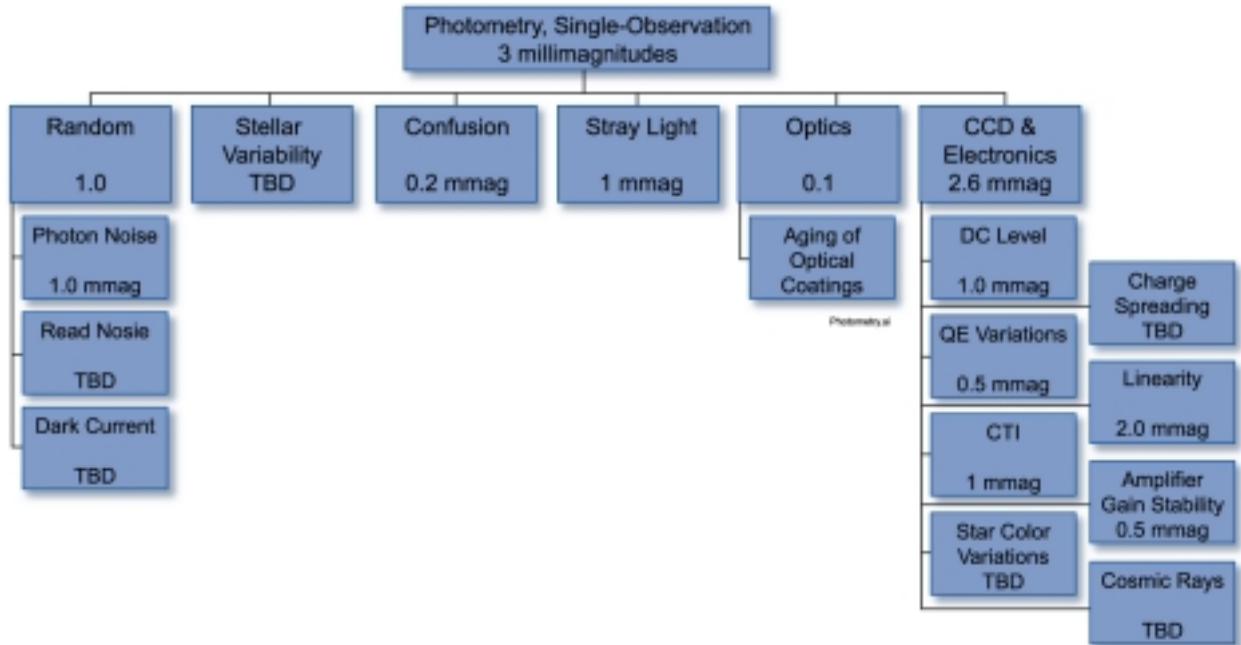


Figure 3-5.

Errors in the determination of the stars apparent brightness in the four Sloan filters for a single observation at $m_v = 9$. Units are millimagnitudes.

3.6 Photometry, Mission.

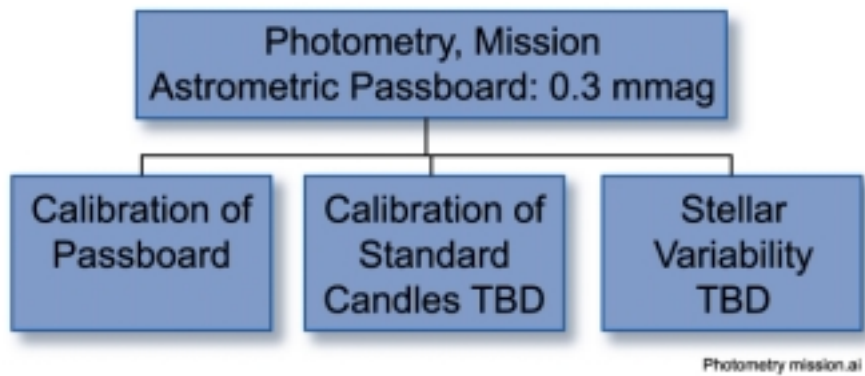


Figure 3-6.

The mission absolute photometric accuracy.

3.7 Data Windows.

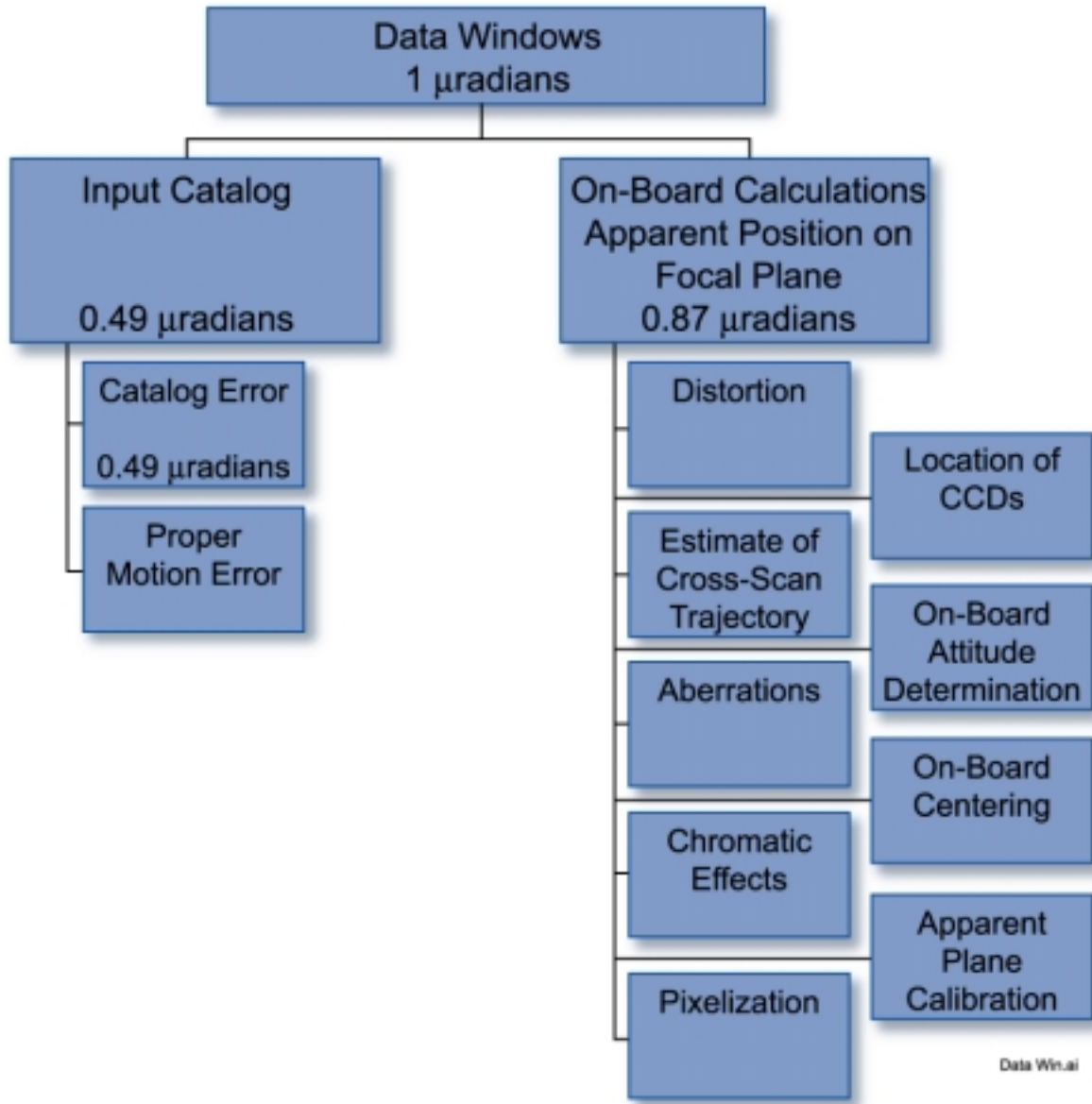


Figure 3–7.

Errors in determining a star's *a priori* position for placing the data windows in the proper location on the CCDs. Units are μradians.

3.8 Acquisition Mode.

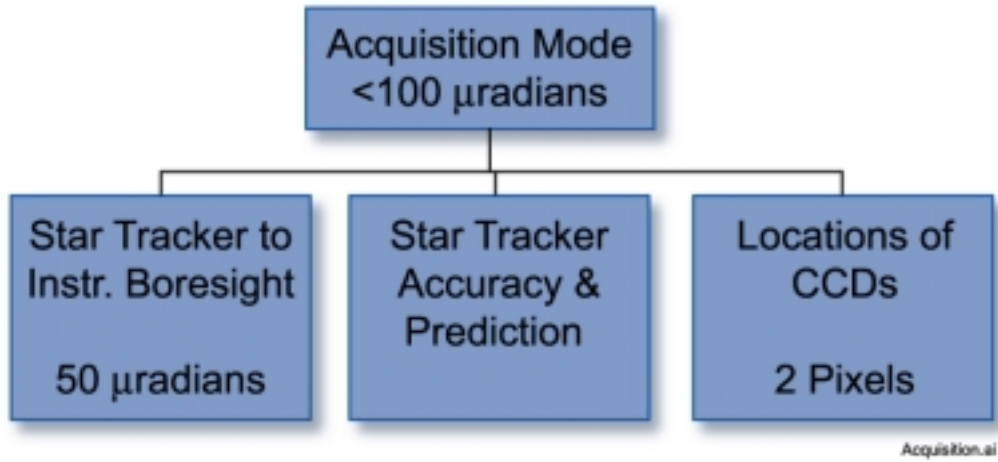


Figure 3-8.

This is a special error budget that only applies to the initial operation of the instrument. The top level of this error tree sets the size of the data windows to be used for acquisition mode.

DRAFT

4. ERROR BUDGET DESCRIPTION

4.1 Science Requirements.

The FAME science requirements are fully described in "*FAME Science Requirements*" and the primary science requirements are repeated in Section 1.2.1 of this document. To achieve these objectives, multiple observations are made of stars over the course of the mission. These individual observations are combined in the ground data analysis pipeline to provide a rigid reference frame (the FAME reference frame).

The astrometry error budget is broken up into two sections, one for single measurements, and one for the astrometric parameters (2 position, 2 proper motion, and parallax) using all mission data. Observations of extragalactic sources by FAME will be necessary to remove a temporal rotation of the FAME frame with respect to a pseudo inertial frame. The final FAME reference frame will be more precise and rigid than any previous celestial frame. All parameters will be with respect to the solar system barycenter. Although many scientific studies will be made using the FAME frame alone, it will be placed on the Celestial Reference System by observation of the optical position of extragalactic radio sources and optical stars that display radio emission for studies of phenomena at other than optical wavelengths.. The FAME frame will most likely be adopted over the present radio ICRF frame if a sufficient number of extragalactic sources are observed by FAME.

The Science Requirements also specify the error for photometry, and an error budget is presented for single-observation and mission photometry errors. The photometry will be measured using the entire bandwidth of the astrometric CCDs and with CCDs covered with four SDSS filters. The photometric data will be specified on a FAME system for the astrometric CCDs and on the SDSS system for the measurements made with the g', r', i', and z' filters.

Requirements are also presented for Cross-Scan Error (which results in entries in the Astrometry, Single-Observation, In-Scan Error tree), for error in placement of Data Windows and for error in Acquisition Mode.

The error trees apply to 9th magnitude stars. For brighter and fainter stars, Table TBD presents the errors with reference to the treatment for V=9 stars.

4.2 Astrometry, Single Observation Error, In-Scan.

The requirement on in-scan accuracy for a single observation is 2.9 nanoradians (590 μ arcsec, 1/350 pixel), *a posteriori* (see below). This accuracy requirement includes the effects of "random" errors, those that are uncorrelated from one passage of the star to another, and "systematic" errors, those that are correlated, i.e., they depend repeatably on one or more particular parameters.

Random error cannot be removed by modeling, and a single expectation value is given for the resulting single observation error. This value will be reduced by the square root of the number of measurements in the mission error. Systematic error may be partly removed by modeling, both in single-observation error and in mission error. For single-observation error, two bounds are given: *a priori* and *a posteriori*. These refer to the error of a single observation before and after modeling (fitting) using iterative least-squares reductions, taking advantage of all mission and ancillary data. The *a posteriori* errors are dominated by photon statistics, and will be largely uncorrelated from one epoch to another.

For example, the error due to PSF variations depends on star color, phase with respect to the pixel, position in the field, blurring due to s/c attitude, etc. A model can be built which is a function of these parameters. Application of the model corrects an *a priori* value, creating an *a posteriori* value. In some cases, for instance that of stellar spectrum, an *a priori* value cannot be obtained in isolation, as the spectrum model is an essential part of the centering process. In those cases, the *a priori* value given is the error that would be obtained with worst-case guesses at the parameters for that model.

The FAME single-error in scan requirement is based on the experience with star centering of CCD data by USNO and LMCO following the publication of the Concept Study Report (6/18/99), and prior to 8/5/99. Performance was better than 1/350 pixel = 2.9 nradian = 590 μ as, with an experimental setup that was not optimized and a CCD that was not science grade. The lower limit to error is set by photon statistics, determined by covariance study (see Sec. 4.2.1), and estimates of the magnitudes of the various systematic error sources (Sec. 4.2.2 through 4.2.7).

4.2.1 Random.

The requirement for errors that are uncorrelated from one observation to another is $1.5 \text{ nradian} = 300 \text{ microarcsec}$.

These estimates come from the SAO covariance study, which determined the centering accuracy possible with a least-square fit, if the functional form of the PSF is known, but not its width. The covariance study does not include systematic errors, which are taken into account in other parts of the error tree. Separate estimates of photon noise, read noise, and dark current are provided. The blurring effect from several sources can be combined by taking the RSS of the rms values of the several blurring effects. This is exactly true for Gaussian blurring functions, but is approximately true for a wide variety of functional forms.

Discussion of the covariance study is available in Optical system for an astrometric survey from space; additional documentation on this and other centering studies is on the FAME web site. The covariance study uses a model of the stellar spectrum, either blackbody, from a Kurucz model or actual stars from the Gunn-Stryker catalog, to generate pseudodata. To generate synthetic observations (CCD readings), it performs a numerical integration over wavelength, and integrates that quantity over the desired pixels. Diffraction, pixel size, and (optionally) charge spreading are taken into account, but imperfections in the optical system are ignored.

Iteration can be performed, resulting in best-fit values for position, image width (blackbody temperature, or position on the main sequence for the Kurucz models), and brightness, with estimates for the formal error of these quantities. For the covariance study, no iteration is performed, yielding only the uncertainty estimates but giving a more comprehensive picture of parameter space. The variation of uncertainty with "pixel phase" (the position within one pixel) is taken into account by averaging the information (qualitatively, the inverse square of uncertainty) over phase. Various combinations, such as real stars modeled with Kurucz or blackbody spectra, have resulted in errors of at most a few millipixels, suggesting that the centroiding process is robust.

4.2.1.1 Photon Noise.

This is the centroiding error due to photon statistics.

4.2.1.2 Read Noise.

The total read noise is $\leq 12.2 \text{ e-}$.

The total read noise value is the sum in quadrature of the read noise from the CCD and the read noise of the electronics. The astrometric error due to total read noise equals that due to photon statistics at $V \sim 15$; at $V=9$ read noise is insignificant.

4.2.1.2.1 CCD Read Noise.

The CCD read noise shall be $\leq 7 \text{ e-}$.

The CCD read noise requirement is derived by extrapolating measured read noise values at read rates slower than the FAME rate. This number will need to be reviewed once a camera system is operational at the FAME data rates.

4.2.1.2.2 Electronics Read Noise.

The electronics read noise shall be $\leq 10 \text{ e-}$.

The post-CCD electronics contribute significant noise because 24 CCD's are packaged in a small space, the electronics must be approximately 1 m from the CCD's, and a high clock frequency must be used (3.3 MHz). It would be desirable to reduce this value, to improve performance on stars of magnitude $V \sim 15$.

4.2.1.3 Dark Current.

The dark current is $2 \text{ e-}/\text{pixel}$.

The astrometric error from dark current is comparable with that due to read noise.

Table 4-1. Blur Sources (TBD)

Description	RMS value	Varies with
Charge spreading, 18 μm FWHM	0.51 μradian	CCD to CCD & ?within one CCD
Jitter (0.01 pixel at 100 Hz)	0.01 μradian	Time
Optical aberration	??	Field position
CCD Clocking (3 clock states, each having equal time)	0.2 μradian	--
TDI error		
Rotation rate determination	??	Time (random, but varies slowly with time, if rotation rate varies slowly)
TDI Rate Setting	0.1 μradian	Time
Oscillator stability	?? (very small)	??
Optical distortion, cubic, 280 ppm at field edge	0.3 μradian	Field position
Cross-scan smear	??	
TOTAL BLUR (RSS)	0.63 μradian	

The net blur is to be convolved with the diffractive PSF, to yield an effective PSF, from which the centroiding precision may be calculated. Total blur is to be no more than 0.63 μradian (0.13 arcsec), and shall not vary from one rotation to the next (TBR) by more than 0.01 μradian (0.002 arcsec) (TBR).

The blurring effect from several sources can be combined by taking the RSS of the rms values of the several blurring effects. This is exactly true for Gaussian blurring functions, but is approximately true for a wide variety of functional forms.

The net blur is used in calculating the Random error estimate. The effect of this blur is equivalent to charge spreading of 21.5 μm . To give best estimates of image widths, which may be important in detecting binaries with overlapping PSF's, it may be important to keep time-variable blur to a minimum. The time-variable blur is probably primarily due to spacecraft jitter.

4.2.1.4 Cosmic Rays.

4.2.2 TDI Error.

The total TDI error is the mismatch of the clock rate of the CCDs and the rotation rate of the spacecraft. The effect is primarily blur, covered in Table 4-1. The error due to the blur is covered in section 4.2.1. There is also a centroid offset error of TBD *a priori* and TBD (very small) *a posteriori*, due to the low frequency component of clock rate mismatch. The total TDI error results from several sources, which are discussed below.

The astrometric offset effect of the clock is similar to in-scan jitter, and is probably accounted for with the same model parameters.

4.2.2.1 Rotation Rate Determination Error.

The error in the instrument's determination of the rotation rate of the spacecraft is TBD.

This will be set by our on-board centering capability.

4.2.2.2 TDI Rate Mismatch.

The total mismatch between the measured rotation rate and the set TDI rate is TBD.

This mismatch is the result of the limited resolution of the TDI settings in the instrument and the effects of drift in the S/C rotation rate.

4.2.2.2.1 TDI Setting Resolution.

The TDI rate error resulting from the limited resolution of the TDI settings is TBD.

This error is set by the fact that the TDI clock is derived from the instrument clock by division by an integer, and there is a practical limit to how high that frequency can be (the effective frequency is 200 MHz).

4.2.2.2.2 S/C Rotation Rate Drift.

This is the (RMS?) difference between the set TDI rate and the ideal TDI rate when the rotation rate changes at maximum permissible amount, and the TDI clock is updated as often as allowed. Since data for stars on the CCDs are lost when the TDI rate is changed, the TDI rate should not be changed frequently. The resulting error is TBD.

4.2.2.3 Oscillator Stability.

The instrument clock shall introduce no more than 0.1 nradian error on time scales of 100 sec and shorter. This is the blur and offset due to the instability of the instrument clock oscillator. Variations in the clock are equivalent to variations of in-scan spacecraft motion, and can be removed in the spiral reduction by a change in the rotation rate model, or perhaps explicit clock parameters may be used. The clock specification can be set more stringently than spacecraft jitter in both frequency and amplitude, because clocks of the required stability are readily available. The clock is required to have the stability specified in Table 4-2. Specifications for one oscillator are given as an example to demonstrate availability, but this does not imply a preference for this brand over others.

Table 4-2. Clock Stability

Time scale	100 sec	1 sec
Angular error	0.1 nradian	0.1 nradian
Req'd root Allan variance	4×10^{-10}	4×10^{-8}
Vectron EMXO	7×10^{-12}	2.4×10^{-12}

4.2.2.4 Optical Distortion.

The blur due to the distortion - variation in magnification over the field - of the telescope system shall be TBD μ radian. The systematic error due to distortion is treated in sections 4.X.X.X and 4.2.7.3.

Optical distortion is primarily a radial shift of the center of the image, a cubic function of radius. The peak shift (at the edge of the field) is TBD ppm. Higher order terms, as well as manufacturing and alignment tolerances, will require estimation of a modest number of parameters across the field of view. These parameters are expected to be moderately stable. They are expected to depend on star color primarily because of the wavelength dependence of diffraction.

Approx peak shift is 280 ppm, unless LMCO has managed to reduce it at all. Reference IRD?

Phillips can provide blur estimate. Approx 0.3 microradian.

4.2.3 Dynamical Perturbations.

Dynamical perturbations result in in-scan and cross-scan motion . These are required to produce an in-scan error of no more than 0.9 nradian, a posteriori.

Dynamical perturbations influence the spacecraft attitude and motion. High frequency motion causes primary blur, and low frequency motion primarily an offset error. Perturbations at frequencies substantially below $f_0 = 1/(1.56 \text{ sec})$ can be removed by modeling the spacecraft motion, but this becomes impossible as the perturbation frequency approaches f_0 . Therefore, in the region of f_0 the specification upon jitter must be the most stringent.

4.2.3.1 Stochastic and Other Hard To Model Dynamical Perturbations.

These perturbations cannot easily be removed from the data via simple physical modeling or bias parameters. Hence, they are potentially the most significant dynamical sources of systematic error.

4.2.3.1.1 Fuel Sloshing.

Attitude perturbations will be caused by fuel sloshing and fuel currents inside the bladder.

The perturbations will have both along-scan and cross-scan effects on the motions of stars across the focal plane. The magnitudes and behavior TBD.

4.2.3.1.2 Earth Radiation Pressure.

Variations in the pressure field incident on the spacecraft due to radiation from the Earth will produce dynamical perturbations.

These variations include both visible and infra-radiation, and are caused by day/night diurnal and annual cycles, latitude and longitude variations due to topography, variations due to weather, and variations due to vegetation cycles. The resulting torques can be complicated because of the bus and instrument geometry, optical ports, and AKM holes. The magnitudes and behavior are TBD.

4.2.3.1.3 Variability of Solar Irradiance.

The solar radiation pressure field incident on the “top side” of the shield will vary at all timescales in the range < 1 min. to > 11 years. Variations include short-term fluctuations that are stochastic and therefore unmodelable, variation on the order of 0.1 percent over long timescales (months to years), and variation on the order of 0.01 percent over short timescales (minutes to hours).

The resulting in-scan error is 27 μas (1 σ) for a cross-scan 1- σ knowledge of 5 mas. The relation is nearly linear:

$$\sigma_s(\mu\text{as}) = -2.8(8) + 5.95(4) \sigma_c(\text{mas}) - 0.0036(4) [\sigma_c(\text{mas})]^2,$$

where σ_s is the standard error in the scan direction in units of $\mu\text{arcseconds}$, and σ_c is the standard error of cross-scan measurements in units of milliarcseconds . This relation was determined by a least squares fit of dynamical simulation results that incorporated 1-minute resolution broadband SoHO data for the solar radiation field, and it holds for σ_c at least in the range 5 to 100 mas.

4.2.3.1.4 This Section Deleted.**4.2.3.2 Solar Shield Dynamical Perturbations.**

Many of these perturbations can be removed from the data via physical modeling and bias parameters.

4.2.3.2.1 Shield (Panels, Teflon Tape, Webbing, Etc.) and Flattop Albedos.

These are dynamical perturbations due to absorption and reflection variations of the surfaces exposed to the solar radiation pressure field. The variations in surface properties are caused by aging of materials, spatial inhomogeneities (spots on the shield), variations in solar cell power draw, and the AKM hole or cover. The magnitudes and behavior are TBD.

4.2.3.2.2 Variations In Effective Shield Angle.

Dynamical perturbations will be caused by asymmetries in the solar shield geometry — namely the variation of the angle at which a tangent plane at a specific point on the shield intersects the spin axis.

The chief effects will be variation of the spin period and excitation of nutation. Ideally, the shield angle is independent of position on the shield. In practice, it will vary, but the effects of the variations are mitigated to some extent by rotational averaging. Specific asymmetries include nonuniform shield angle as a function of circumference, slow variation over time, and fast variation – flapping modes – that may be excited by internal or external forces. The magnitudes and behavior are TBD.

4.2.3.2.3 Shield Component Geometry Perturbations.

Dynamical perturbations will be caused by any non-flatness of the components of the “solar shield”.

Description:

- solar panels

- ◆ potato chipping
- ◆ dynamical modes
 - radial (flapping)
 - twisting
 - what are the timescales for damping?
- interpanel membranes
 - ◆ sagging
 - ◆ flapping

Magnitude of effect: Magnitudes and behavior TBD.

4.2.3.2.4 Thermal Radiation Emission Torques.

Torques due to thermal radiation by the spacecraft will produce dynamical perturbations. Sources of thermal radiation include radiation from viewports, reradiation of incident solar flux, (re)radiation from the underside of the shield, and radiation from instrument heat exhaust thermal radiators. The magnitudes and behavior are TBD.

4.2.3.2.5 Axis of Shield Misaligned With Spacecraft Spin Axis.

This is composed of two components: (1) misalignment of the circumferentially averaged shield axis with respect to the spacecraft instrument + bus symmetry axis and (2) misalignment of the instrument + bus symmetry axis with respect to the total angular velocity vector (spin + precession). The magnitudes and behavior are TBD.

4.2.3.2.6 This Section Deleted.

4.2.3.3 Dynamical Perturbations Due To Isolated Events.

These perturbations are due to isolated events, some of which are predictable and some of which are not. The events will cause breaks in the data stream. The effects may be mitigated by the use of Kalman filters. Detailed simulations will be required in order to quantitatively determine the severity of the event types.

4.2.3.3.1 Eclipses.

Eclipses of solar radiation due to Earth's shadow have the potential to excite various dynamical modes, especially in the solar shield. The severity will depend on mode amplitudes and damping times. The magnitudes and behavior are TBD.

4.2.3.3.2 Geotail Particle Bursts.

As the spacecraft orbits within the Earth's magnetosphere, the particle flux levels will vary. These fluxes act as pressure perturbations that will affect the spacecraft spin dynamics. Very large bursts can occur from fast CME events, typically a few times per year around solar max. The magnitudes and behavior are TBD.

4.2.3.3.3 Magnetopause Crossings.

Dynamical perturbations will result when the spacecraft crosses the magnetopause (the boundary between the Earth's magnetosphere and the solar wind). These events are relatively rare at geosynch (a few times a year), and produce a short duration (typically ~15 min) exposure to full solar wind. The magnitudes and behavior are TBD, but may be quite large since the solar wind pressure is three orders of magnitude larger than the solar radiation pressure.

4.2.3.3.4 Micrometeoroid Hits.

Impact of micrometeoroids on the spacecraft can produce perturbations.

The magnitudes and behavior are TBD.

4.2.3.4 Other Smooth Dynamical Perturbations.

The effects of these perturbations can largely be removed from the data via modeling and bias parameters. Therefore, the magnitudes of these effects can be substantially larger than those in 4.2.3.1.

4.2.3.4.1 Precession Variation.

Due to unperturbed precession of the spin axis around the nominal direction of the Sun, the motion of a star across the focal plane will vary sinusoidally with the spin phase. To lowest order, there is no in-scan motion, but there is a large cross-scan motion. In-scan motions are present at second order.

In the cross-scan direction, the first-order image motion has a maximum rate of 4.0 pixels over one CCD crossing time (1.56 sec). The period of the motion is 40 minutes (one spin period). The second-order motion is a rotational velocity field. The cross-scan component of the second-order field has a maximum amplitude of 1/27 of a pixel (7.6 mas) at the edge of the FOV, and a period of 40 minutes (one spin period). Its magnitude is a function of distance from the center of the FOV. The third-order component is very small — 1/40,000 of a pixel = 5 μas — and a complicated function of time and position.

In the in-scan direction, the first-order image motion is constant. This component changes the spin period by 2.36 seconds. The second-order motion is again due to the second-order rotational velocity field. The along-scan component of the second-order field has a maximum amplitude of 1/27 of a pixel (7.6 mas) at the edge of the FOV, and a period of 40 minutes (one spin period). Its magnitude is a function of distance from the center of the FOV. The third-order component is again very small -- 1/40,000 of a pixel = 5 μas

4.2.3.4.2 Stellar Aberration Variation.

As the spacecraft spins, the viewport direction on the sky changes with respect to the projected direction of travel of the Earth in its orbit. Hence, there will be a sinusoidal variation of aberration with spin phase. The aberration variation will produce smear of up to 1/1000 pixel (= 220 μas), over one CCD crossing, toward projected direction of Earth orbital motion (the source of the spacecraft acceleration).

4.2.3.4.3 Gravity Gradient Torques.

Torques will result from mass asymmetries of the spacecraft interacting with gravitational field gradients. The primary component is the usual gravity gradient torque due to the diagonal elements of the moment of inertia tensor and the Earth's gravitational field gradient. Secondary components due to off-diagonal terms of the moment of inertia tensor are equivalent to a misalignment of the spacecraft symmetry axis with respect to the spin axis. The result is a modulation of the precession with a 24 hour period (the orbital period of the spacecraft). The magnitude of the effect depends on the ratio of inertia moments.

Assuming the current baseline mass properties for the s/c and instrument (mass = 550 kg, effective length of spacecraft = 2 m, $I_x = 349 \text{ kg m}^2$, and $I_z/I_x = 0.81$), the worst-case amplitude of the sinusoidal signal, which depends on orientation of s/c with respect to the Earth, is 0.183 arcsec/sec in the precession rate.

To find the cross-scan component, multiply by $\sin \theta \cos \phi = \frac{1}{\sqrt{2}} \cos \phi$, where θ is the spin phase and ϕ is the Sun angle. The resulting worst-case cross-scan component of the precession perturbation due to the worst-case 24-hour gravity gradient torque is $\frac{0.183}{\sqrt{2}} \text{ arcsec/sec} = 1.0 \text{ pixels per 1.56 seconds}$.

The worst-case along-scan component of that worst-case signal is $\frac{0.183}{\sqrt{2}} = 1.0 \text{ pixels per 1.56 seconds}$. As the s/c orbits Earth, the precession variation will cross zero 6 hours after the worst-case point, go to worst case amplitude in the opposite direction in 6 more hours, cross zero 6 hours after that, and repeat.

Therefore, the smear due to the dominant gravity gradient effect on the current s/c is a maximum of 1 pixel per 1.56 second in both focal plane directions. Note that the cross-scan signal is sinusoidal on the period of the fast Euler angle θ (i.e., the spin phase). That period is $1 / (1/40 \text{ min}^{-1} \cos \psi) = 40.039 \text{ min}$ (i.e., essentially the spin period). The along-scan signal has just the 24 hour period. Thus, we have

$$\begin{bmatrix} \Delta c \\ \Delta s \end{bmatrix} = \Omega_\varphi \cos\left(\frac{2\pi}{24hr \cdot t} + \alpha_1\right) \begin{bmatrix} \cos\left(\frac{2\pi}{40 \text{ min} \cdot t} + \alpha_2\right) \\ 1 \end{bmatrix}$$

where $[\Delta c, \Delta s] = [\text{cross-scan smear}, \text{scan-direction smear}]$, $\Omega_\varphi = 1.0 \text{ pixel}/1.56 \text{ sec}$, α_1 and α_2 are arbitrary phase angles.

The precession perturbation amplitude Ω_φ can be calculated from:

$$\Omega_\varphi = \frac{1}{2} \frac{(1-\gamma)}{(2-\gamma)} \left(\frac{2\pi}{T}\right)^2 L^2 \frac{m}{I_z \Omega_\theta} \cos \varphi$$

where $\gamma = \text{ratio of moments} = I_z / I_x$, $T = \text{orbital period} = 24 \text{ hrs}$, $L = \text{effective length of spacecraft (it's modeled}$

here as a constant-density cylinder), $m = \text{spacecraft mass}$, and $\Omega_\theta = \frac{2\pi}{\text{spinperiod}} = \frac{2\pi}{40 \text{ min}}$.

This analysis assumed a symmetric spacecraft, so in real life there will be motions due to $I_x / I_y \neq 1$ on timescales of the spin period, as well as other motions due to the non-sphericity of the actual Earth gravity field. Presumably these motions are all much smaller than the dominant effect.

4.2.3.4.4 Magnetic Torques.

Torques will arise due to the interaction of the Earth's magnetic field with electrical currents in the spacecraft. The magnitudes and behavior are TBD.

4.2.3.4.5 Movement of Center of Gravity As Fuel is Expended.

The magnitudes and behavior are TBD, but can be made small with movement of trim masses.

4.2.3.4.6 Variations of Instantaneous Sun Direction Due to sun Tracking Dynamics.

The angle between the spin axis and sun direction will vary by 3-5 degrees over the course of 1-3 weeks, due to sun-tracking dynamics. The impact on various spin dynamics considerations are TBD.

4.2.3.4.7 Variation of Solar Radiation Pressure As Spacecraft Orbits Around the Earth.

The effects of solar pressure variation over the Earth orbit are TBD. It is anticipated that they will be small.

4.2.3.4.8 Lunar, Solar, and Planetary Gravitational Torques.

The gravitational torques produced by sources other than the Earth are expected to be small. Their effects are TBD.

4.2.4 This section intentionally blank.

4.2.5 PSF Knowledge.

4.2.5.1 Stellar Spectrum.

???

This is the error due to the fact that stars differ in color and thus have differently shaped PSFs.

4.2.5.2 Start-Stop Technology ($V < 9$).

This is any excess error that results from centering on the "string of pearls" images generated by Start-Stop Technology, to be used for stars with $5 < V < 9$. The excess error may be reduced to insignificance when fitting is done with a model of the bright star images with trails between. The trails do become relatively more significant for brighter stars, both because the contrast ratio between image and trail decreases, and because photon noise is diminished in importance, so that higher precision is possible.

Error for stars of V other than 9 is handled in Table TBD; there we find quantitative departures from the $V=9$ case. The error due to SST is the only qualitatively new error source for a star of another magnitude, so it has an entry in the Single-Observation tree.

4.2.5.3 Optical Effect on PSF.

This is the effect of aberrations such as coma on the shape of the PSF. It is a function of position in the field of view, but varies slowly through the mission, the fastest variation being possible changes due to thermal changes in the structure. The relevant a posteriori value is after modeling. Even a symmetrical change of shape, if not modeled with adequate fidelity, will cause an error if, as is usually the case, the star is not at the edge or center of the pixel. The error due to change of shape of PSF due to optical aberrations is TBD.

4.2.5.4 Confusion.

Some companions will be resolved, or partly resolved, so that by eye they can be recognized. This technique can be automated and extended to much smaller separations by studying the variation of apparent image width along the scan direction as a function of observation angle. In idealized studies, width variations of 1%, ~ 2 milliarcsec, have been detected from the data of a single observation (at 7.5 m focal length). In practice, it will be more difficult, but the ~ 1000 observations over the mission will help, as will the finer sampling with the 15 m focal length. Other companions will be detected by studying the fit positions as a function of time through the mission, which will depart from straight-line motion because of an orbit. The error due to confusion, i.e., one or more additional stars near the subject star, with overlapping PSF's, is TBD nradian.

4.2.6 Spacecraft Tracking.

Spacecraft tracking will yield a velocity model with 1 cm/sec error. This produces the a priori error of 0.034 nradian. The spiral solution will improve this to $< \sim 0.005$ nradian. (In the spiral solution, errors in projected velocity may be estimated directly, or aberration may be removed by absorbing it into the spacecraft rotation model.) Note that the astrometric error depends only on the s/c velocity knowledge error, not on the velocity itself.

4.2.6.1 Unmodeled Velocity Perturbations.

The error due to unmodeled velocity perturbations is TBD. Unmodeled velocity perturbations are not expected to limit the accuracy of the velocity model.

4.2.6.2 S/C Position Knowledge.

The S/C position knowledge shall contribute an error of < 50 nradians ($10 \mu\text{s}$).

The a priori knowledge of the position of the S/C is required with respect to the solar system barycenter. The displacement of an observed star depends on the stellar parallax which is the inverse of the barycentric distance. This is the S/C to ground station distance plus the position of the ground station with respect to the solar system barycenter. For a parallax of 1 arcsecond and an error of $10 \mu\text{arcseconds}$, the S/C barycentric distance must be known at the level of 10^{-6} AU or 150 km. This requirement is not expected to present any difficulty. At this time the Earth's orbit is known with a relative accuracy of 10^{-8} .

4.2.6.3 This Section Deleted.

4.2.6.4 Time Knowledge.

The knowledge of UT at the ground station shall contribute < 50 nradians ($10 \mu\text{s}$).

The timing knowledge requirement is set by the spiral reduction, aberration correction and the Earth ephemeris. The absolute knowledge of the time of star images is one millisecond. This will contribute an error of <50 nrad ($10 \mu\text{as}$).

4.2.7 Optics.

4.2.7.1 Stray Light.

4.2.7.1.1 Earth.

4.2.7.1.2 Moon.

4.2.7.1.3 Bright Stars/Planets.

4.2.7.1.4 Sun.

4.2.7.1.5 Other Background.

4.2.7.2 Aberration, Including Distortion.

4.2.7.3 Opto-Thermal-Mechanical Stability.

4.2.7.4 Chromatic Errors.

4.2.8 CCD and Electronics.

This category of errors relates to the effects intrinsic to the Charged Coupled Devices (CCD'S) used as the FAME detectors as well as the Poisson noise intrinsic to all photon detectors.

The overall requirement on the in-scan determination of the star centers relative to nearby stars is to a precision of 2.5 nanoradians ($510 \mu\text{as}$).

This requirement is set based on the experience with star centering of CCD data by USNO and LMCO following the publication of the Concept Study Report (6/18/99), and prior to 8/5/99. Performance was better than $1/350$ pixel = 2.9 nradian = $590 \mu\text{as}$, with an experimental setup that was not optimized and a CCD that was not science grade.

4.2.8.1 Charge Spreading.

The rms blur corresponding to a charge spreading of $18 \mu\text{m}$ FWHM ($1.2 \mu\text{radian}$ FWHM) is $0.51 \mu\text{radian}$ (105 arcsec). The extent of charge spreading for FAME CCD's is not known yet, and may be much smaller.

This is the dominant blurring term (see Table TBD). The value given is from "RGO Technical Note 118: The Measurement of Spatial Resolution in EEV4280 CCD Images". The spreading will vary from chip to chip, and perhaps (gradually) within a chip, as the charge spreading depends on whether the CCD is operating fully depleted, which depends on thinning. The extent of thinning can vary over a chip.

4.2.8.2 Charge Transfer Inefficiency (CTI).

Charge Transfer Inefficiency is defined as $\text{CTI} = 1 - \text{CTE}$, where CTE is the Charge transfer Efficiency. The FAME CCDs shall have a CTI less than $1\text{E-}6$ at end of life after 5 years in orbit. This CTI will produce an a priori error of less than TBD nrad, and an a posteriori error of less than TBD nrad.

As the FAME CCDs are exposed to the radiation environment in space, the CTI will change from a uniform low value (except for "bad" pixels) to a distribution of traps. Many of the traps will have a capacity of a single electron, but up to half of the damage is caused by nuclear interactions, which concentrate many traps in a small number of neighboring pixels. CTI is a function of signal strength; large charge packets see more traps than small packets, approximately in proportion to the square root of the number of electrons in the packet.

Without mitigation, the CTI would cause large astrometric errors, and could prevent the detection of stars at the faint limit. Mitigating the traps is the function of the "fat zero" charge injection ahead of each star image. With fat zero, the residual CTI is TBD.

Modeling the CTI on a column-by-column basis presents a significant computational challenge. In principal, however, the modeling should be feasible because CTI is expected to change primarily during a small number of solar flares, which are of short duration and independently identifiable. Between flares, a column will observe many $V = 9$ stars. A complication is that precession smearing exposes pieces of several columns to a given star.

It will be possible to bound CTI errors adequately only after testing on an irradiated CD that is capable of injecting "fat zero" charge. Useful auxiliary information may be obtained upon an irradiated CCD not capable of injecting charge.

4.2.8.3 Wavelength Dependence of Absorption.

Wavelength dependence of absorption in the CCD causes an error of no more than TBD nradians.

Away from the center of the field of view, the beam impinges on the CCD at non-normal incidence (the exit pupil is ~ 3.5 m from the detector). A redder star's light penetrates further, causing the star to appear to be closer to the edge of the field. A priori, the effect is TBD nradians, but it is expected to be a stable function of the stellar spectrum and position in the field, so will require estimation of a modest number of parameters over the mission.

4.2.8.4 Quantum Efficiency Variation.

The error in centering due to Quantum Efficiency (QE) variations is TBD.

CCDs typically have color dependent variations in their quantum efficiency, which varies from pixel to pixel. The row to row variation, and intra-pixel variation in the scan and direction, will be averaged away by TDI, except for any portion which is sensitive to the voltages on the electrodes, so moves with the image. The QE variation from column to column in TDI mode should be significantly reduced from normal CCD operation due to the averaging over CCD rows.

4.2.8.5 Amplifier Gain Stability.

The amplifier gain stability has to be 0.1% over 40 minutes. See section 4.5.1.6.7.

4.2.8.6 Linearity.

Deviation of $<5\%$ linearity over the range 4000 – 40,000 e^- . See section 4.5.1.6.6.

4.3 Unbinned Cross-Scan Motion.

The requirement on control of cross-scan motion is $9 \mu\text{rad}$ in 1.56 sec. The requirement marked "knowledge" is a requirement that centering in the cross-scan direction on the unbinned stars used as guide stars produce a result accurate to 24 nradian (5 milliarcsec) on each star.

With respect to ... the reference frame of the instrument? We are using information from one port to determine attitude, which tells us about field rotation in the other port. We probably need another requirement here, which has to do with torsional stability of the two fields of view. Relates to cross-scan angle, for one thing.

This number is 5 milliarcsec from one $V=9$ star, which is ample accuracy, as I recall from Marc Murison's study [this is true, 5 mas cross-scan knowledge limits in-scan error due to solar irradiance fluctuations to $\sim 30 \mu\text{s}$ — MAM]. The peak rotation error is at the edge of the FOV, 0.55 deg. The product of 0.55 deg and 5 mas is $50 \mu\text{s}$, adequately small.

4.3.1 Dynamical Perturbations.

4.3.1.1 Stochastic and Other Hard-to-Model Dynamical Perturbations.

These perturbations cannot easily be removed from the data via simple physical modeling or bias parameters. Hence, they are potentially the most significant dynamical sources of systematic error.

4.3.1.1.1 Fuel Sloshing.

See 4.2.3.1.1.

4.3.1.1.2 Earth Radiation Pressure.

See 4.2.3.1.2.

4.3.1.1.3 Variability of Solar Irradiance.

Definition: Intrinsic variation of the solar radiation pressure field incident on the “top side” of the shield.

Description: See 4.2.3.1.3.

Magnitude of effect: Cross-scan perturbations of stars at the focal plane are roughly 0.03-0.10 arcsec (0.05 arcsec is a typical average amplitude) with period of order the spin period and an amplitude envelope timescale of order several hours. This variation is due mainly to excitation of nutation by the irradiance fluctuations. These numbers are based on simulations that incorporate SoHO 1-minute resolution irradiance data and nutation damping with a half-amplitude decay time of ~9 hours.

4.3.1.1.4 Nutation Damping Mechanism Stiction and/or Other Undesirable Behaviors.

See 4.2.3.1.4.

4.3.1.2 Solar Shield Dynamical Perturbations.

Many of these perturbations can easily be removed from the data via physical modeling and bias parameters.

4.3.1.2.1 Shield (Panels, Teflon Tape, Webbing, Etc.) and Flattop Albedos.

See 4.2.3.2.1.

4.3.1.2.2 Variations In Effective Shield Angle.

See 4.2.3.2.2.

4.3.1.2.3 Shield Component Geometry Perturbations.

See 4.2.3.2.3.

4.3.1.2.4 Thermal Radiation Emission Torques.

See 4.2.3.2.4.

4.3.1.2.5 Axis of Shield Misaligned With Spacecraft Spin Axis.

See 4.2.3.2.5.

4.3.1.2.6 This Section Deleted.**4.3.1.3 Dynamical Perturbations Due to Isolated Events.**

These perturbations are due to isolated events, some of which are predictable and some of which are not. The events will cause breaks in the data stream. The effects may be mitigated by the use of Kalman filters. Detailed simulations will be required in order to quantitatively determine the severity of the event types.

4.3.1.3.1 Eclipses.

See 4.2.3.3.1.

4.3.1.3.2 Geotail Particle Bursts.

See 4.2.3.3.2.

4.3.1.3.3 Magnetopause Crossings.

See 4.2.3.3.3.

4.3.1.3.4 Micrometeoroid Hits.

See 4.2.3.3.4.

4.3.1.4 Other Smooth Dynamical Perturbation.

These perturbations can largely be removed from the data via modeling and bias parameters.

4.3.1.4.1 Precession Variation.

See 4.2.3.4.1.

4.3.1.4.2 Aberration Variation.

See 4.2.3.4.2.

4.3.1.4.3 Gravity Gradient Torques.

See 4.2.3.4.3.

4.3.1.4.4 Magnetic Torques.

See 4.2.3.4.4.

4.3.1.4.5 Movement of Center of Gravity As Fuel Is Expended.

See 4.2.3.4.5.

4.3.1.4.6 Variations of Instantaneous Sun Direction Due to Sun Tracking Dynamics.

See 4.2.3.4.6.

4.3.1.4.7 Variation of Solar Radiation Pressure As Spacecraft Orbits Around the Earth.

See 4.2.3.4.7.

4.3.1.4.8 Lunar, Solar, and Planetary Gravitational Torques.

See 4.2.3.4.8.

4.3.2 Random.

4.3.3 Cross-Scan Jitter.

Jitter is defined as motion that is not modelable. The excitation of cross-scan jitter by dynamical perturbations (cf. section 4.2.3) shall be less than TBD.

4.3.4 Optics.

See Section 4.2.7.

4.3.4.1 Stray Light.

See Section 4.2.7.1.

4.3.4.1.1 Earth.

See Section 4.2.7.1.1.

4.3.4.1.2 Moon.

See Section 4.2.7.1.2.

4.3.4.1.3 Bright Stars/Planets.

See Section 4.2.7.1.3.

4.3.4.1.4 Sun.

See Section 4.2.7.1.4.

4.3.4.1.5 Other Background.

See Section 4.2.7.1.5.

4.3.4.2 Optical Distortion.

See Section 4.2.7.2.

4.3.4.3 Other Optical Aberrations.

See Section 4.2.7.2.

4.3.4.4 Opto-Thermal-Mechanical Stability.

The requirement on rotation of one viewport with respect to the other is TBD nradian over TBD minutes. Refer to section 4.2.7.3.

4.3.4.5 Chromatic Errors.

Refer to section 4.2.7.4.

4.3.5 CCD and Electronics.

Refer to section 4.2.8.

4.3.5.1 Photon Noise.**4.3.5.2 Read Noise.**

The read noise data is $\leq 12.2 e^-$.

The read noise of the CCD is estimated by extrapolating measured read noise values at read rates slower than the FAME rate. This number will need to be reviewed once a camera system is operational at the FAME data rates.

4.3.5.2.1 CCD Read Noise.

The CCD read noise at the FAME rate shall be $\leq 7e^-$.

CCD SOW. The read noise of the CCD is estimated by extrapolating measured read noise values at read rates slower than the FAME rate. This number will need to be reviewed once a camera system is operational at the FAME data rates.

4.3.5.2.2 Electronics Read Noise.

The CCD electronics read noise at the FAME rate shall be $\leq 10e^-$.

Estimate from Earl.

4.3.5.3 Quantum Efficiency Variation.

The error in centering due to QE variations is TBD.

CCD's typically have color dependent variations in their quantum efficiency from pixel to pixel. The QE variation from column to column in TDI mode should be significantly reduced from normal CCD operation due to the averaging over CCD rows.

4.3.5.4 Charge Transfer Inefficiency (CTI).

The Charge Transfer Inefficiency

CTI is a much easier problem for cross-scan than it is for in-scan centering. To first order, only the traps in the serial register affect cross-scan. There are fewer of these (mean number of columns crossed is 512), and they all affect all

the stars, except that the stars only go through part of the SR. Fat zero mitigates SR traps as well: the FZ bar goes out through the SR. Also, the centering requirement is less demanding than for in-scan.

The Charge Transfer Inefficiency more commonly referred to in terms of the Charge Transfer Efficiency (CTE) [CTI=1-CTE], however, since the CTE of modern CCD'S is often of order 0.999995, it is easier to express in terms of the CTI. As the FAME CCD'S are exposed to a radiation environment in space, the CTI will change from a uniform low value (except in "bad" pixel) to a distribution of discrete traps. The value quoted above is for the value of the CTI at the end-of-life after 5 years in orbit.

4.3.5.5 Dark Current.

4.3.5.6 Star Color Variation.

???

This is the error due to the fact stars differ in color and thus have different shaped PSFs.

4.3.5.7 Charge Spreading.

The error in the centering in the in-scan direction due to charge spreading in the CCD is TBD.

4.3.5.8 Amplifier Gain Stability.

4.3.5.9 Linearity.

4.3.5.10 Cosmic Rays.

4.4 Astrometry, Mission.

The requirement upon final positions is 0.24 nradians = 50 μ arcsec. Error in this class is averaged single-observation error, random and systematic, with an allowance for correlations in the systematic error that causes it no to average to zero.

4.4.1 Number of Observations.

4.4.1.1 Confusion.

The data windows telemetered from the instrument to the ground are sized to maximize the science data returned, thus are as small as possible. The requirement is that the peak of a target star's PSF be contained in the central 4 pixels of the 10×20 pixel windows (see § 4.7 of this document). When the image of a secondary star falls within the data window associated with a particular target star (stellar confusion) it is anticipated that centroiding of the target star may be adversely effected due to overlap of the two stellar PSFs. The magnitude of the effect of stellar confusion on target star centroiding will depend upon the relative brightness of target and secondary stars, their actual separation, and the particular centroiding algorithms chosen for data reduction and analysis. From statistical confusion studies based on the USNO A2.0 Catalog it is estimated that on average, approximately 6% of target star observations will be contaminated by secondary stellar images (16.0^m to 19.0^m range) falling in the target star data window. When considering brighter stars (9.0^m to 15.0^m range) the average contamination falls to less than 1%. The number of observations lost due to stellar confusion is TBD from future studies employing a more realistic data simulator and data analysis techniques.

4.4.1.2 Eclipses.

The number of observations rejected due to Observatory instability during and after eclipses by the Earth is TBD.

???

Eclipse occur in 17% of orbits, and last up to 67 minutes. We require astrometric data to be taken through as much of the eclipse phase as possible with minimal disturbance to the S/C motions. The degree of S/C instability resulting from eclipses by the Earth is TBD. The resulting impact on the number of observations is TBD.

4.4.1.3 Occultations.

The fraction of observations rejected due to the Earth or Moon being in either viewport (Earth/Moon occultation) is 1.1%. The degree of S/C instability and length of the recovery period resulting from occultation by the Earth or Moon is TBD. The resulting impact on the number of observations is TBD.

4.4.1.4 Bright Stars/Scattered Light.

The number of observations rejected due to a bright star or other point source being placed in the field of view is TBD (see § 4.4.1.1 above). The number of observations rejected due to photons from nearby bright stars and other objects being scattered into the focal plane is TBD, depending upon TBR instrumental parameters.

4.4.1.5 Cosmic Rays.

The number of observations rejected due to cosmic ray hits near the star is TBD.

???

4.4.1.6 Bad Columns.

4.4.2 Scanning Geometry.

4.4.2.1 Nominal Sun Angle.

The table below shows the percentages of the sky for which a 2.5 year FAME mission can meet or exceed the goals of 50 μ s (position, parallax) and 50 μ s/yr (proper motion), for three nominal Sun angles, assuming a 580 μ s single-measurement standard error. Proper motion in longitude fails for any reasonable Sun Angle. (A longer mission remedies this failure.) The parallax requirement then restricts the nominal Sun angle to ≥ 43 degrees.

	45 degrees	40 degrees	35 degrees
parallax	98	79	65
position – longitude	100	86	58
position - latitude	100	100	100
pm – longitude	54	43	33
pm - latitude	100	100	100

4.4.2.2 Precession Rate.

A 2.5 year mission with 45 degree nominal Sun angle and 580 μ s single measurement standard error can meet the goals of 50 μ s (position, parallax) and 50 μ s/yr (proper motion) over 90% of the sky or better (except for proper motion in longitude, as noted above) for any precession period in the range 15-30 days. The mission astrometric parameter errors are insensitive to precession period in the stated range. Generally, a shorter precession period is preferred over a longer precession period, but the effect on mission accuracies is slight. Mission accuracies appear to start breaking down around 30 days, indicating that 30 days is an upper limit to the precession period.

4.4.2.3 Spin Rate.

The table below shows the percentages of the sky for which a 2.5 year FAME mission can meet or do better than the goals of 50 μ s (position, parallax) and 50 μ s/yr (proper motion), for three spin periods (35, 30, and 45 minutes), nominal Sun angle 45 degrees and assuming a 580 μ s single-measurement standard error. Proper motion in longitude fails for spin periods in the range of 35-45 minutes. The parallax requirement then restricts the spin period to ≤ 43 minutes.

	35 minutes	40 minutes	45 minutes
parallax	100	98	86
position – longitude	100	100	98
position - latitude	100	100	100
pm – longitude	62	54	48
pm - latitude	100	100	98

4.4.3 Single-Observation Error.

See section 4.2.

4.4.4 Optics.

4.4.4.1 Basic Angle Stability.

The basic angle stability shall be 0.05 radians over intervals of 10 minutes.

4.4.4.1.1 Compound Mirror Stability.

TBD

4.4.4.1.2 Twisting of Other Optical Elements.

TBD

4.4.5 S/C Tracking.

See section 4.2.6.

4.4.5.1 S/C Position.

See section 4.2.6.2.

4.4.5.2 Gound Station Position.

See sections 4.2.6.2 and 4.2.6.3.

4.4.5.3 Time Knowledge.

See section 4.2.6.4.

4.4.6 Instrument Parameter Calibrations.

This is residual systematic error after calibration with all mission data, and after averaging over the mission.

4.5 Photometry, Single Observation.

4.5.1 Photometry Using Astrometric CCDs.

The photometric accuracy requirement for a star of magnitude 9 on the astrometric chip for a single observation is 3 mmag. This arises from:

Photon Noise:	1.0 mmag
DC Level:	1.0 mmag
QE Variations:	0.5 mmag
Confusion:	0.2 mmag (nongaussian)
Amp Stability:	0.5 mmag

Linearity:	2.0 mmag
Charge Traps:	1? mmag (nongaussian)
Stray Light:	1? mmag (nongaussian)

The sources of this error are discussed below.

4.5.1.1 Random.

4.5.1.1.1 Photon Noise.

Photon noise error will depend on the number of photons detected by the FAME CCDs. For a 9th magnitude star, 900,000 electrons will be produced in the astrometric CCDs, yielding an error of 1 mmag. The total signal for the CCDs will depend upon the integration time for a single observation. The present integration time of 1.56 seconds is for the baseline design using neutral density filters to observe bright stars. If start stop technology is used to observe the bright stars, then the integration time for these stars would be less than 1.56 seconds. See section 4.2.1.1

4.5.1.1.2 Read Noise.

The photometric error due to read noise is TBD.

4.5.1.1.3 Dark Current.

The photometric error due to dark current is TBD.

4.5.1.2 Stellar Variability.

The variability of stellar optical emission will not affect the single measurement accuracy unless the emission exceeds the gain setting for the observation.

4.5.1.3 Confusion.

Confusion produces a radiometric error when a faint star in one aperture contaminates a star that is being observed in the other aperture. We can check for contamination by using a catalog like USNO-A for stars down to mag~19. The resulting photometric error is TBD.

4.5.1.4 Stray Light.

Stray Light will change the apparent sky background level. Observing blank sky "stars" will detect this. This effect should be slowly varying so about one measurement per frame will be enough to follow it. Glints are to be avoided. The resulting photometric error is TBD.

4.5.1.5 Optics.

Variation in the performance of the optics, such as aging of the coatings, will degrade the throughput of the optical system. The resulting photometric error is TBD.

4.5.1.5.1 Aging of Optical Coatings.

See 4.5.1.5.

4.5.1.6 CCD and Electronics.

These effects are those contributed by the CCDs and electronics.

4.5.1.6.1 DC Level.

This corresponds to an error of 1 DN in the DC determination. This accuracy must be achieved in 2 ways: (1) putting blank sky "stars" in the input catalog and observing them like real stars, and (2) reading the CCD overscan about 10 times per frame for each gain setting and for binned and unbinned data, and reporting to the ground the mean values with other data each frame. For the relatively few stars in nebulosity with real sky, the sky value will have to be solved for.

Note that THE ONBOARD CCD CONTROL SOFTWARE MUST BE ABLE TO READ AND REPORT THE OVERSCAN periodically for each gain setting and for binned and unbinned data.

4.5.1.6.2 Quantum Efficiency Variations.

The specifications for the CCDs should limit the effect of quantum efficiency variations to 1.0 mmag at magnitude=9.

4.5.1.6.3 CTI Effects.

The photometric error due to CTI is TBD.

4.5.1.6.4 Star Color Variation.

The photometric error due to star color variation is TBD.

4.5.1.6.5 Charge Spreading.

The photometric error due to charge spreading is TBD.

4.5.1.6.6 Linearity.

This error depends on how linear the CCDs and electronics are, and how stable the system linearity is. The CCD specifications require <5% deviation from linearity over the range 4000-40000 e⁻. The linearity will be measured on the ground. In flight, the linearity must be checked by observing selected stars with several different stop/start integration times, and/or observing selected stars with two gain settings. The former method is preferable.

Note that the onboard CCD control software must be able to read selected stars with different stop/start integrations or with different gain settings.

4.5.1.6.7 Amplifier Gain Stability.

The amplifier gain is required to stable to 0.1% over 40 minutes.

4.5.1.6.8 Charge Traps.

Charge traps have the potential to dominate the photometric errors as they get worse toward the end of the mission. At the beginning of the mission, traps will be few, and the data with traps will appear as outliers in the average of any one star.

Traps that release charge quickly will release the charge inside the data acquisition window where it can be measured. Such traps will degrade astrometry before they degrade photometry.

4.5.2 Photometry Using SDSS Filters.

The single measurement observation in the SDSS filters will have a photon noise of 1.6 mmag. The other effects contributing to the error are the same as the astrometric filters, giving a single measurement accuracy of 3.2 mmag.

4.5.3 Sloan Filters.

The single measurement observation in the Sloan filters will have a photon noise of 1.6 mmag. The other effects contributing to the error are the same as the astrometric filters, giving a single measurement accuracy of 3.2 mmag.

4.6 Photometry, Mission.

4.6.1 Photometry Using Astrometric CCDs.

The effects of photon noise, DC level, QE variations, and amplifier stability and linearity will be reduced by the square root of the number of observations if the calibration of the observations is performed as described above. These calibrations include the measurement of the DC level, and amplitude stability and linearity by taking frequent measurements of blank sky stars, reading the CCD overscan for each CCD at 1.5 second intervals and by observing several stars with different start/stop integration times or by observing stars with two different gain settings. Those effects that contribute in a non-gaussian way to the observations must be reduced to a minimum. Confusion may be

identified in the data by inspection of catalogs for stars of magnitude 19 and brighter that will appear in the observation window. These data can be removed or fitted for multiple sources. The effect of stray light may be removed if it is slowly varying, however, 'glints' will affect the data. The effect of charge traps has not been examined. If we assume these non-gossip effects are not present in 75% of the data, and can be removed, then 600 observations will reduce the error in the overall average measurement to 0.15 mmag

The photometric measurements will be placed on an instrumental system by adopting those stars whose intensities are constant as calibrators. Those calibrators for the astrometric CCDs will be selected from the stars observed. This will be an iterative procedure.

4.6.1.1 Calibration of Standard Stars.

Standard stars will be adapted for the astrometric CCDs. The SDSS photometric system has established standard stars. These stars will be observed by FAME and used to transfer the FAME precision photometry onto the SDSS system.

4.6.1.2 Stellar Variability

4.6.2 Photometry Using SDSS Filters.

As before the error contribution to the photometry is identical in the SDSS filter with the exception of the reduced bandwidth and the placing of the observed stars on the SDSS standard system. There will be adequate SDSS standard stars between magnitudes 10-13 for transformation onto the SDSS system. The precision of the photometry for of order 25 measurements will be 0.6 mmag. In converting this onto the SDSS system, it is estimated that the accuracy will be 1 mmag. SDSS standard stars will be observed by the FAME mission. These stars will be employed to place the photometry onto the SDSS system. The primary source of error in this transformation will be a mismatch of the FAME filter passbands and the SDSS standard passbands. Therefore, each of the FAME filters must have turn-on and turn-off wavelengths (measured at the 50% transmission that agree with the SDSS standard passbands within 5% and that remain stable within 5% for the duration of the mission

4.6.2.1 Standard Candles.

See section 4.6.2.1.

4.6.2.2 Ground Calibration of Passbands.

4.6.2.3 Stellar Variability.

4.6.3 Sloan Filters.

As before the error contribution to the photometry is identical in the Sloan filter with the exception of the reduced bandwidth and the placing of the observed stars on the Sloan standard system. There will be adequate Sloan standard stars between magnitudes 10-13 for transformation onto the Sloan system. The precision of the photometry for of order 25 measurements will be 0.6 mmag. In converting this onto the Sloan system, it is estimated that the accuracy will be 1 mmag. The primary source of error in this transformation will be a mismatch of the FAME filter passbands and the Sloan standard passbands. Therefore, each of the FAME filters must have turn-on and turn-off wavelengths (measured at the 50% transmission that agree with the Sloan standard passbands within 5% and that remain stable within 5% for the duration of the mission.

4.7 Data Windows.

The data windows telemetered from the instrument to the ground are sized to maximize the science data returned, thus are as small as possible. The requirement is that the peak of the star's PSF be contained in the central 4 pixels of the 13 (along scan) by 20 (cross scan averaged) pixel windows for normal operations. This also applies to the unbinned data on 9th magnitude stars taken for the attitude determination of the Observatory. The star's position is required to fall within one pixel of its predicted value on the focal plane.

4.7.1 Input Catalog.

The input catalog is required to be accurate to $0.49 \mu\text{radians}$ (0.1 arcsec) at the time of the observation in ICRF coordinates. This corresponds to 0.5 pixels on the FAME CCDS. This number is determined by the accuracy of the UCAC catalog and by the CCD pixel size projected on the sky of $1 \mu\text{radian}$.

4.7.1.1 Catalog Error.

The error in the catalog position at the epoch of observation will contribute to the error of the input catalog. This position must be transformed to the time of the FAME observation via the stars position in the catalog and its proper motion and parallax. The apparent position at the time of the FAME observation must be within 0.1 arcsecond of the position of the star.

4.7.1.2 Proper Motion Error.

See section 4.7.1.1. In order to maintain the apparent positions of the objects observed by FAME, the on board catalog will have to be updated for high proper motion objects, minor planets and targets of opportunity..

4.7.1.2.1 Proper Motion in the Catalog Epoch.

In order to calculate the position of an object at the time of a FAME observation, proper motion must be taken into account. One contribution is the proper motion used in the making the catalog that is transforming the stars position at time observation to the epoch of the catalog. Further, there is the error that enters into the position when transforming the position from the epoch of the catalog to the time of the FAME observation.

4.7.1.2.2 Proper Motion in the Current Epoch Relative to the Catalog Epoch.

See section 4.7.1.2.1.

4.7.2 On-Board Calculation.

The on-board calculation of the star's position on the focal plane shall be accurate to $0.87 \mu\text{radians}$. This requires that the apparent position of the object observed take account of the aberration caused by the Observatory's motion with respect to the solar system barycenter. The Observatory's velocity vector must be known in real time to 1.5 km/s . For the observation of solar system objects such as minor planets, the position of the spacecraft must be known in real time to 150 km .

4.7.2.1 Distortion.

The distortion of the optics will shift the apparent positions of the stars in both the scan and the cross scan direction. The effects of this distortion must be predictable to 0.05 pixels in both coordinates.

4.7.2.2 Estimates of Cross-Scan Trajectory.

The on-board software will need to estimate the cross-scan trajectory of the star across the CCD to ensure that the data window is centered on the center of the smeared PSF.

4.7.2.3 Aberrations.

Other optical aberrations may cause an offset in the apparent centers of the stars.

4.7.2.4 Chromatic Effects.

The offsets in the star's position may depend on the color of the star.

4.7.2.5 Pixelization.

The discrete nature of the pixels may have TBD effects.

4.7.2.6 Location of the CCDs.

The on-board knowledge of the CCD locations must be sufficiently accurate to allow the prediction of the star locations.

4.7.2.7 On-Board Attitude Determination.

The error in the on-board attitude determination shall be 0.5 (TBD) μ radian.

4.7.2.8 On-Board Centering.

4.8 Acquisition Mode.

These are the errors associated with the proper function of acquisition mode, which is where the attitude knowledge of the Observatory is passed from the S/C bus to the instrument. The top level requirement of 100 μ radians is set by the size of the acquisition windows used by the instrument. This is for acquisition and prediction. The size of the acquisition window is 200 by 200 pixels.

4.8.1 Star Tracker to Instrument Boresight.

The knowledge of the star tracker boresight relative to the FAME telescope boresight is 50 μ rad or 10".

4.8.2 Star Tracker Accuracy.

The accuracy of the star tracker shall be 50 μ radians (10 arcsec).

4.8.3 Locations of CCDs.

Initial locations of the CCD'S from pre-flight measurements shall be known to 2 μ radians TBR ($\pm 30 \mu$ m on the focal plane).

DRAFT

5. NOTES

5.1 Definitions.

Basic Angle	The angle between the two telescope fields of view measured in a plane perpendicular to the symmetry axis of the space vehicle.
Blocked Column	Columns in which a blockage or trapping are sufficiently severe in the CCD during the manufacturer's characterization that low-level signal charge cannot be transferred out regardless of the applied level of charge injection. Such columns should be readily apparent during Fe55 testing.
Charge Injection	Columns in which charge transfer efficiency is good (normal) as determined by Fe55 testing, Blocked Columns and optical response is good (normal) at any level of illumination, but the level of charge injection is diminished by 5% relative to the response of undiminished columns. Such columns are detectable only by applying a charge injection.
Cross-scan	The direction perpendicular to that of motion on the focal plane of stars in the fields of view due to the Observatory's rotation.
Dark Column	Columns in which no charge transfer defects are present, but optical response integrated over the length of the column is diminished by 5%, measured at 50% FW, relative to the mean response of undiminished columns. Such columns will not be apparent during Fe55 testing, and require optical stimulation. Such columns presumably result from an optical defect in the surface or anti-reflection (AR) coatings of the CCD.
Distortion	Classical optical aberration that occurs when the magnification or plane scale changes with position in the field. The distortion in the FAME system is negative, which gives a barrel distortion. As stars approach the edge of the field in the scan direction, they will appear to slow down.
Hot Columns	Columns in which charge is generated in the absence of optical stimulation which exceeds $20e^-$.
Observatory	The FAME observatory is defined as the integrated space vehicle including the instrument, spacecraft bus, and Sun shield/solar arrays.
Partially Blocked	Columns in which blockage of charge takes place only after a threshold signal level is exceeded, but in which charge transfer is normal for signal levels less than that threshold. Such columns should not be apparent during Fe55 testing, and will require high-level optical stimulation to be detected.
Scan	The direction of motion on the focal plane of stars in the fields of view due to the Observatory's rotation.
Spacecraft	Generally refers to the spacecraft bus only, but could be in reference to the entire Observatory
Sun angle	The instantaneous angle between the S/C symmetry axis and the direction of the Sun.
TBD	To Be Determined. The use of this term implies an "open" requirement issue which must be resolved prior to CDR.
TBR	To Be Released/To Be Resolved. The meaning should be clear in the context of the use. In both cases the use of this term implies an "open" requirement issue which must be resolved prior to CDR.
Trapped Columns	Columns in which one or more low-level traps are present in the CCD.

5.2 Acronyms and Abbreviations.

μas	Microarcseconds
BC	Blocked Column
CCD	Charge Coupled Device
CIBC	Charge Injection Blocked Columns
CTE	Charge transfer efficiency
CTE	Coefficient of thermal expansion
CTI	Charge transfer inefficiency
DC	Dark Column
DoD	Department of Defense
EEE	Electrical, Electronic, and Electromechanical
ESD	Electrostatic Discharge
FAME	Full-sky Astrometric Mapping Explorer
FOV	Field of View
HC	Hot Columns
ICD	Interface Control Document
ICRF	International Celestial Reference Frame
IRD	Instrument Requirements Document
MAR	MIDEX Assurance Requirements
MIDEX	Medium Class Explorer
MRD	Mission Requirements Document
NASA	National Aeronautics and Space Administration
NSDS	NASA Software Documentation Standard
PBC	Partially Blocked Columns
RSS	Root Sum Square
S/C	Spacecraft
SRD	Science Requirements Document
TC	Trapped Columns
TDI	Time Delay Integration, a.k.a. drift scan. An technique for operating the CCDs where the charge on the CCD is clocked down the columns of the image area at the same rate an image moves across the CCD.
TBD	To Be Determined.
TBR	To Be Released/To Be Resolved

